Published OnlineFirst September 9, 2011; DOI:10.1158/1078-0432.CCR-11-0313

Clinical Cancer Research

Expression of *NLRR3* Orphan Receptor Gene Is Negatively Regulated by MYCN and Miz-1, and Its Downregulation Is Associated with Unfavorable Outcome in Neuroblastoma

Jesmin Akter, Atsushi Takatori, Md. Shamim Hossain, et al.

Clin Cancer Res 2011;17:6681-6692. Published OnlineFirst September 9, 2011.

Published OnlineFirst September 9, 2011; DOI:10.1158/1078-0432.CCR-11-0313

Clinical Cancer Research

Expression of *NLRR3* Orphan Receptor Gene Is Negatively Regulated by MYCN and Miz-1, and Its Downregulation Is Associated with Unfavorable Outcome in Neuroblastoma

Jesmin Akter[1,2], Atsushi Takatori[1], Md. Shamim Hossain[1], Toshinori Ozaki[1,3], Atsuko Nakazawa[5], Miki Ohira[4], Yusuke Suenaga[1], and Akira Nakagawara[1,2]

Abstract

Purpose: Our previous study showed that expression of NLRR3 is significantly high in favorable neuroblastomas (NBL), whereas that of NLRR1 is significantly high in unfavorable NBLs. However, the molecular mechanism of transcriptional regulation of *NLRR3* remains elusive. This study was undertaken to clarify the transcriptional regulation of *NLRR3* and its association with the prognosis of NBL.

Experimental Design: *NLRR3* and *MYCN* expressions in NBL cell lines were analyzed after induction of cell differentiation, MYCN knockdown, and overexpression. The transcriptional regulation of *NLRR3* was analyzed by luciferase reporter and chromatin immunoprecipitation assays. Quantitative PCR was used for examining the expression of *NLRR3*, *Miz-1*, or *MYCN* in 87 primary NBLs.

Results: The expression of *NLRR3* mRNA was upregulated during differentiation of NBL cells induced by retinoic acid, accompanied with reduced expression of *MYCN*, suggesting that *NLRR3* expression was inversely correlated with *MYCN* in differentiation. Indeed, knockdown of *MYCN* induced *NLRR3* expression, whereas exogenously expressed MYCN reduced cellular *NLRR3* expression. We found that Miz-1 was highly expressed in favorable NBLs and *NLRR3* was induced by *Miz-1* expression in NBL cells. MYCN and Miz-1 complexes bound to *NLRR3* promoter and showed a negative regulation of *NLRR3* expression. In addition, a combination of low expression of *NLRR3* and high expression of *MYCN* was highly associated with poor prognosis.

Conclusions: *NLRR3* is a direct target of MYCN, which associates with Miz-1 and negatively regulates *NLRR3* expression. NLRR3 may play a role in NBL differentiation and the survival of NBL patients by inversely correlating with *MYCN* amplification. *Clin Cancer Res; 17(21); 6681–92. ©2011 AACR.*

Introduction

Neuroblastoma (NBL) is one of the most common malignant solid tumors in children and accounts for 8% of all pediatric cancers (1). NBLs originate from sympathetic precursor neuroblasts derived from the neural crest. NBLs found in patients older than 1 year are usually aggressive and eventually kill the patients despite intensive therapy, whereas those in patients younger than 1 year often regress spontaneously or maturate, resulting in a favorable prognosis (2). We have made extensive efforts to show that TrkA, a high-affinity receptor for nerve growth factor, and TrkB, a receptor for brain-derived neurotrophic factor as well as neurotrophin 4/5, are important key regulators (3–6). However, the precise molecular mechanisms of how NBL becomes aggressive and how the spontaneous regression is induced still remain elusive.

Amplification of the *MYCN* oncogene is strongly associated with rapid progression of NBL (7). The *MYCN* amplification occurs in approximately 25% of NBL and is one of the most important prognostic indicators of poor clinical outcome (8–12). MYCN is a nuclear transcription factor and its expression level is well associated with cell proliferation of NBL cells (13, 14). In general, MYCN exerts its biological functions through transcriptional regulation of its target genes in both positive and negative manners. MYCN has an ability to activate its target genes by forming a heterodimer with MAX and binds to the E-box motif, CACGTG, in the proximal promoter region (15–18). On the contrary, MYCN represses the expression of genes, such

Authors' Affiliations: [1]Division of Biochemistry and Innovative Cancer Therapeutics, Chiba Cancer Center; [2]Department of Molecular Biology and Oncology, Chiba University Graduate School of Medicine; [3]Laboratories of Anti-Tumor Research and [4]Cancer Genomics, Chiba Cancer Center Research Institute, Chiba; and [5]Department of Pathology, National Center for Child Health and Development, Tokyo, Japan

Note: Supplementary data for this article are available at Clinical Cancer Research Online (http://clincancerres.aacrjournals.org/).

Corresponding Author: Akira Nakagawara, Division of Biochemistry and Innovative Cancer Therapeutics, Chiba Cancer Center, 666-2 Nitona, Chuoh-ku, Chiba 260-8717, Japan. Phone: 81-43-264-5431; Fax: 81-43-265-4459; E-mail: akiranak@chiba-cc.jp

doi: 10.1158/1078-0432.CCR-11-0313

Published OnlineFirst September 9, 2011; DOI:10.1158/1078-0432.CCR-11-0313

Translational Relevance

Amplification of *MYCN* oncogene is strongly associated with rapid progression of neuroblastoma (NBL) and one of the most important prognostic indicators of poor clinical outcome. Our group previously reported that NLRR3 is highly expressed in a favorable subset of NBL but until this work, there was no sound investigation of the function of NLRR3 and its transcriptional regulation. In this study, we found that *NLRR3* is a direct target of MYCN but its expression is negatively regulated by MYCN in association with Miz-1. Furthermore, a combination of low expression level of *NLRR3* and high expression level of *MYCN* was strongly correlated with the poor prognosis. These data suggest that the expression pattern of NLRR3, Miz-1, and MYCN plays an important role in defining the clinical behavior of NBLs. The decreased expression of NLRR3 might be one of the key events regulating the aggressive behavior of NBL.

as $p15^{INK4b}$, $p21^{CIP1}$, and *NDRG2*, when it forms a complex with transcriptional regulators, such as Myc-interacting zinc finger protein 1 (Miz-1) and Sp1 (19–21). Koppen and colleagues have previously described that MYCN suppresses *Dickkopf-1* (*DKK1*) expression, resulting in proliferation of NBL cells (22). However, the precise mechanism of how MYCN contributes to NBL aggressiveness remains unclear.

We have identified human neuronal leucine-rich repeat (NLRR) family genes as one of the differentially expressed genes between favorable and unfavorable NBLs, using our unique NBL cDNA libraries (23, 24). The NLRR protein family consists of 3 members, NLRR1, NLRR2, and NLRR3 (23), and belongs to the type *y* transmembrane protein with leucine-rich repeat (LRR) domains containing 11 or 12 LRRs, an immunoglobulin c2-type domain, and a fibronectin type III domain in its extracellular region. The amino acid sequences of NLRR family proteins are highly conserved in the extracellular domains, and NLRR1 and NLRR3 also possess a conserved stretch of 11 amino acids with 2 clathrin adapter interaction domains and a dileucine-type domain in the short intracellular region (25, 26), which might provide a basis for NLRR function. Our previous reports showed that NLRR1 is a direct transcriptional target of MYCN and that a high expression level of *NLRR1* mRNA is associated with a poor prognosis of NBL (23, 27). However, the function of NLRR3 is poorly understood except that mouse *NLRR3* expression is increased in the cerebral cortex after a cortical brain injury (28) and that rat NLRR3 may be involved in the regulation of EGF receptor signaling through interaction with clathrins (26).

We have previously reported that high levels of *NLRR3* mRNA expression are associated with favorable prognostic factors in NBL (23). In this study, we found that NLRR3 is induced during differentiation of NBL cells. Transcriptional analysis has revealed that NLRR3 is a direct transcriptional target of MYCN, which negatively transactivates it in association with Miz-1. Furthermore, high expression of *NLRR3* or *Miz-1* and the combination of high expression of both *NLRR3* and *Miz-1* are significantly associated with a favorable outcome of NBL. On the contrary, the low expression levels of *NLRR3* and high expression of *MYCN* were strongly correlated with a poor prognosis of NBL.

Materials and Methods

Patient population

Eighty-seven patients with NBL were diagnosed clinically and histologically, using a surgically removed tumor specimen according to the International Neuroblastoma Pathological classification (INPC). According to the International NBL Staging System (INSS; ref. 29), 18 patients were diagnosed as stage 1, 11 were stage 2, 20 were stage 3, 33 were stage 4, and 5 were stage 4S. Cytogenetic and molecular biological analysis of all tumors was also carried out by assessing DNA ploidy, *MYCN* amplification, and *TrkA* expression. The patients were then treated following the protocols proposed by the Japanese Infantile NBL Cooperative Study (30) and Group for Treatment of Advanced NBL (31), and subjected to survival analysis of the result in a follow-up period of at least 36 months (range, 4–58). The study was conducted under internal review board approval with appropriate informed consent.

Cell lines and transient transfection

Human NBL-derived cell lines, including SK-N-BE, CHP134, IMR32, GOTO, KAN, KP-N-NS, LAN-5, NB-1, NB-9, NLF, RTBM1, SK-N-DZ, TGW, NB69, NBL-S, OAN, SK-N-AS, SK-N-SH, and SH-SY5Y cells were obtained from the CHOP cell line bank (Philadelphia, PA) and maintained in a culture condition, using RPMI 1640 supplemented with 10% heat-inactivated FBS (Invitrogen), 100 IU/mL penicillin, and 100 μg/mL streptomycin in a 37°C, 5% CO_2 incubator. For the NBL cell differentiation experiment, RTBM1 and SH-SY5Y cells were exposed to all-*trans* retinoic acid (ATRA; Sigma) at a final concentration of 5 μmol/L. For transient transfection, cells were transfected with the indicated expression of plasmids by using a Lipofectamine 2000 transfection reagent (Invitrogen), according to the manufacturer's recommendations.

RNA extraction and semiquantitative reverse transcriptase PCR

Total RNA was prepared from fresh-frozen tissues of primary NBLs or cultured cells by using Trizol reagents (Life Technologies) or the RNeasy Mini kit (Qiagen). Reverse transcription was carried out by random primers and Superscript II (Invitrogen), following the manufacturer's instructions. After reverse transcription, the resultant cDNA was subjected to PCR-based amplification. The sequence of the primer sets were used for PCR amplification is listed in the Supplementary Table S4. All PCR amplifications were carried out with a GeneAmp PCR 9700 (Perkin-Elmer Co), using rTaq DNA polymerase (Takara).

Published OnlineFirst September 9, 2011; DOI:10.1158/1078-0432.CCR-11-0313

The expression of *GAPDH* was measured as an internal control.

Quantitative real-time PCR

cDNA from primary NBLs and cell lines were subjected to the real-time PCR to quantitate the expression levels of *MYCN*, *Miz-1*, and *NLRR3* mRNA. TaqMan GAPDH control reagent kit (Perkin-Elmer Applied Biosystems) was used for *GAPDH* expression and analyzed by an ABI prism 7500 Sequence Detection System (Applied Biosystems). *NLRR3* and *Miz-1* TaqMan probes were purchased from Applied Biosystems. *MYCN* mRNA expression was measured by the SYBR green real-time PCR system. The primers and probes used for real-time PCR were listed in Supplementary Table S4.

Generation of a specific antibody against NLRR3

The rabbit polyclonal anti-NLRR3 antibody was raised against a mixed synthetic peptide corresponding to amino acid sequences between positions 655 to 670 and 692 to 707 of human NLRR3. The peptide and polyclonal antibody (TB0266) were generated by Medical and Biological Laboratories (Nagoya, Japan). The specificity of the affinity-purified antibody was assayed by immunoblotting.

Plasmid constructs

The protein-coding region of *Miz-1* was amplified by PCR and inserted into the *Eco*RI site of pcDNA3.1 (Invitrogen) flanked with a Flag tag. The human *NLRR3* promoter region and its 5′ progressive deletion mutant were amplified by PCR and then inserted into the *Sacy* site in the upstream of the luciferase gene of the pGL3-basic plasmid (Promega). All constructs were verified by DNA sequencing. The pUHD-MYCN vector was kindly provided by Dr. M. Schwab (German Cancer Research Center, Heidelberg, Germany).

Luciferase reporter assay

SH-SY5Y cells were seeded at a density of 5×10^4 cells/12-well cell culture plate and allowed to attach overnight. The cells were transiently cotransfected with each mutant of the human *NLRR3* promoter-driven luciferase reporter and an internal control vector for *Renilla* luciferase, or a combination of the indicated expression vectors. The total amount of plasmid DNA per transfection was kept consistent with the pcDNA3.1 vector. Both firefly and *Renilla* luciferase activities were assayed with the Dual-Luciferase reporter assay system (Promega) according to the manufacturer's instructions. The firefly luminescence signal was normalized on the basis of the *Renilla* luminescence signal.

siRNA transfection

To knockdown endogenous MYCN expression, SK-N-AS, SK-N-BE, and SH-SY5Y cells were transfected with 10 nmol/L of the indicated siRNA purchased from Dharmacon by using LipofectAMINE RNAiMAX (Invitrogen), according to the manufacturer's recommendations. The list of siRNA sequences used will be provided upon request. Forty-eight hours after transfection, cell lysates were prepared and analyzed for the expression levels of NLRR3 and MYCN by immunoblotting.

Immunoblot analysis

The cells were washed twice with ice-cold PBS and then lysed immediately with SDS sample buffer containing 10% glycerol, 5% β-mercaptoethanol, 2.3% SDS, and 62.5 mmol/L Tris-HCl (pH 6.8). The protein concentrations were determined by using Bio-Rad protein assay dye reagent (Bio-Rad Laboratories). Equal amounts of cell lysates were separated by SDS-PAGE and electrophoretically transferred onto Immobilon-P membranes (Millipore). The transferred membranes were blocked with 5% nonfat dry milk in TBS containing 0.1% Tween-20 and incubated with appropriate primary antibodies at room temperature for 1 hour followed by incubation with horseradish peroxidase–conjugated goat anti-mouse or anti-rabbit secondary antibodies (Cell Signaling Technology Inc.) at room temperature for 1 hour. Immunoreactive bands were visualized by an ECL system (GE Healthcare). The primary antibodies used in this study were as follows: monoclonal anti-MYCN (Ab-1; Oncogene Research Products), polyclonal anti-NLRR3, polyclonal anti–Miz-1 (Santa Cruz Biotechnology), monoclonal anti-GAP43 (9-1E21; Chemicon), and polyclonal anti-actin (20-33; Sigma) antibodies.

Chromatin immunoprecipitation assays

A chromatin immunoprecipitation (ChIP) assay was carried out according to the protocol provided by Upstate Biotechnology (Charlottesville). In brief, cells were cross-linked with 1% formaldehyde in medium for 10 minutes at 37°C. Chromatin solutions were prepared and immunoprecipitated with the following antibodies: anti-MYCN, anti–Miz-1, anti-Max rabbit polyclonal antibodies (Santa Cruz Biotechnology), and normal mouse or rabbit serum as a control. The immunoprecipitates were eluted with 100 μL of elution buffer (1% SDS and 1 mmol/L $NaHCO_3$). Formaldehyde-mediated cross-links were reversed by heating at 65°C for 4 hours, and the reaction mixtures were treated with proteinase K at 45°C for 1 hour. DNAs of the immunoprecipitates and control input DNAs were purified by using a QIAquick PCR purification kit (Qiagen). Purified DNA was subjected to optimized semiquantitative PCR amplification protocol for NLRR3 gene promoter and control regions, using appropriate primer sets (Supplementary Table S4).

Statistical analysis

Student *t* tests were employed to examine the possible association between *NLRR3* expression and other prognostic factors. The classification of high and low levels of *NLRR3*, *Miz-1*, and *MYCN* expression was determined on the basis of the mean value obtained from quantitative real-time PCR analysis. Kaplan–Meier survival curves were calculated, and survival distributions were compared by using the log-rank test. Cox regression models were used to search associations along with *NLRR3* expression, *MYCN*

Published OnlineFirst September 9, 2011; DOI:10.1158/1078-0432.CCR-11-0313

expression, *Miz-1* expression, age, *MYCN* amplification status, INSS, *TrkA* expression, DNA index, origin, and survival. Statistical significance was considered if P value was less than 0.05. The statistical analysis was carried out by SPSS Statistical Software release 12.0.

Results

NLRR3 is upregulated during neuronal differentiation

It has been previously reported that the NBL cell lines exposed to ATRA undergo neuronal differentiation (32), accompanied by a marked decrease in the expression levels of *MYCN* (33). To examine the possible involvement of MYCN in the regulation of NLRR3 expression, the NBL-derived RTBM1 cells were treated with or without 5 μmol/L ATRA. As previously described (34), RTBM1 cells underwent neuronal differentiation with extensive neurite outgrowth in response to ATRA treatment (Fig. 1A). The induced differentiation was confirmed by the expression levels of *GAP43*, a marker of neuronal differentiation (35), which increased after ATRA treatment at both mRNA and protein levels (Fig. 1B and C). As expected, MYCN expression was significantly decreased after ATRA treatment and almost diminished at 6 days after treatment. Consistent with our previous observations (23), *NLRR3* was markedly upregulated at the mRNA and protein levels during the differentiation process. Similar results were also obtained from ATRA-treated SH-SY5Y cells (Supplementary Fig. S1A and B).

Inverse correlation between *MYCN* and *NLRR3* expressions

To further confirm a possible relationship between MYCN and NLRR3, we used MYCN-inducible SHEP21N cells originally derived from NBL (36) and treated with tetracycline to switch off the expression of MYCN. As shown in Fig. 2A, the reduced expression level of *MYCN* upon tetracycline treatment was confirmed by reverse transcriptase PCR (RT-PCR) and immunoblotting, whereas NLRR3 expression was increased after tetracycline treatment.

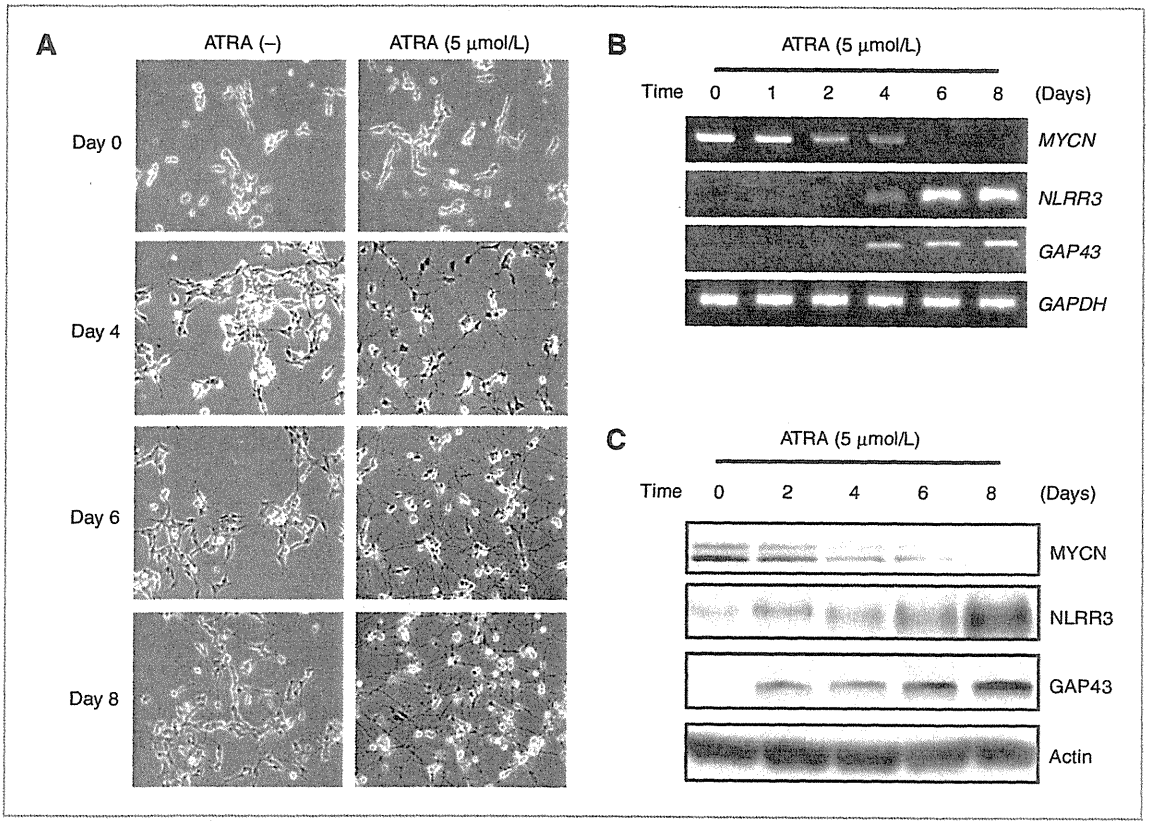

Figure 1. Opposite expression pattern of *NLRR3* and *MYCN* in differentiated RTBM1 cells in response to ATRA. A, ATRA-induced differentiation program in RTBM1 cells. Cells were treated with 5 μmol/L ATRA or left untreated. At the indicated time-periods after treatment with ATRA, neurite outgrowth was examined with a phase-contrast microscope. B and C, RT-PCR and immunoblot analysis for MYCN, NLRR3, and GAP43 in response to ATRA. RTBM1 cells were treated as in A. Total RNA and cell lysates were prepared and processed for RT-PCR (B) and immunoblotting with indicated antibodies (C). For RT-PCR, *GAPDH* was used as an internal control. For immunoblotting, actin was used as a loading control.

Published OnlineFirst September 9, 2011; DOI:10.1158/1078-0432.CCR-11-0313

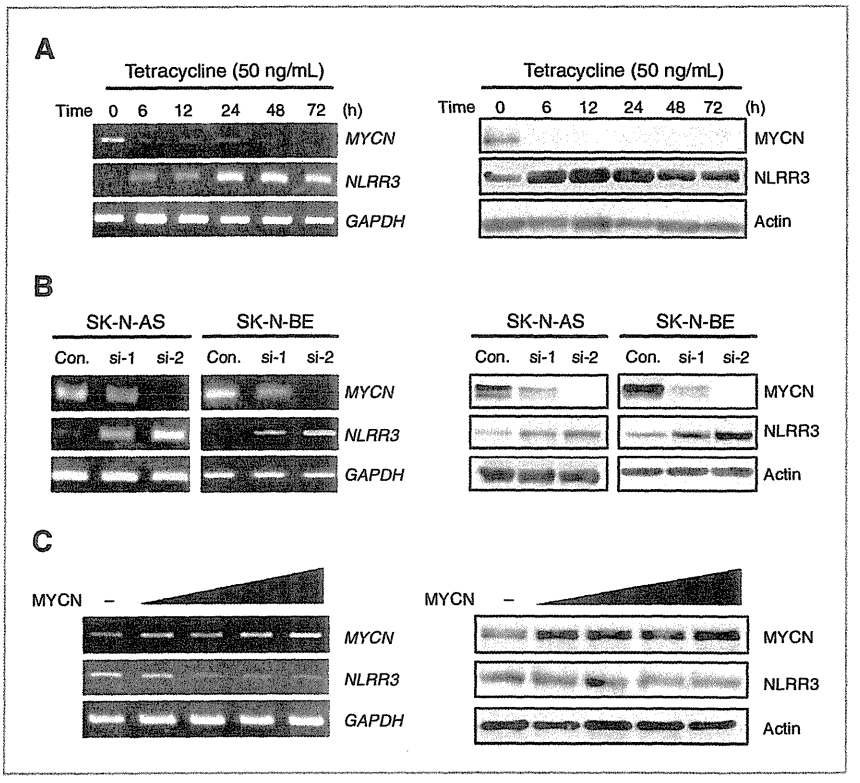

Figure 2. Inverse regulation of MYCN and NLRR3 in various NBL cell lines. A, RT-PCR and immunoblot analysis for MYCN and NLRR3 in SHEP21N cells maintained in the presence of tetracycline. At the indicated time points after the addition of tetracycline (50 ng/mL), total RNA and cell lysates were prepared and processed for RT-PCR (left) and immunoblotting with indicated antibodies (right). B, siRNA-mediated knockdown of the endogenous MYCN. SK-N-AS and SK-N-BE cells were transfected with control siRNA (Con.) or with 2 siRNA (si-1 and si-2) against MYCN. At 48 hours after transfection, total RNA and cell lysates were prepared and processed for RT-PCR (left) and immunoblotting with indicated antibodies (right). C, SH-SY5Y cells were transiently transfected with or without the increasing amounts of the expression plasmid encoding MYCN. Forty-eight hours after transfection, total RNA and cell lysates were prepared and processed for RT-PCR (left) and immunoblotting (right) with indicated antibodies. *GAPDH* was used as an internal control of RT-PCR and actin was used as a loading control for immunoblotting.

To examine whether MYCN and NLRR3 have an inverse functional relationship under these physiologic conditions, siRNA knockdown of the endogenous MYCN was carried out in 2 NBL cell lines, SK-N-AS cells with a single copy of *MYCN* and SK-N-BE cells with *MYCN* amplification. As shown in Fig. 2B, one of the siRNAs against *MYCN*, si-2, efficiently reduced endogenous expression of *MYCN* in both cell lines and resulted in an increased expression of NLRR3. SH-SY5Y cells with a single copy of *MYCN* also showed the similar result after siRNA-mediated knockdown of the endogenous MYCN (Supplementary Fig. S2A and B). These observations prompted us to examine whether MYCN can directly downregulate *NLRR3* expression. To address this issue, SH-SY5Y NBL cells were transfected with the expression plasmid encoding the *MYCN* gene. Forced expression of MYCN resulted in a dose-dependent decrease of NLRR3 expression both at the mRNA and protein levels (Fig. 2C), suggesting that *NLRR3* expression is negatively regulated by MYCN in NBL cells.

MYCN represses the promoter activity of *NLRR3* in association with Miz-1

According to the previous reports (19, 20, 37), Myc proteins repress its target genes by forming a complex with Miz-1. Under these conditions at low expression levels of Myc, Miz-1 activates transcription of the target genes by cooperating with other transcriptional cofactors and enhances cell differentiation (20). Therefore, we hypothesized that Miz-1 might be involved in the regulation of *NLRR3* expression. To prove this, we examined whether exogenously expressed Miz-1 upregulates *NLRR3* expression in SH-SY5Y cells. Figure 3A, left shows that *NLRR3* expression was upregulated by overexpression of Miz-1 in the same manner as a positive control, $p15^{Ink4b}$ expression, whereas expression of other NLRR family members, *NLRR1*

Published OnlineFirst September 9, 2011; DOI:10.1158/1078-0432.CCR-11-0313

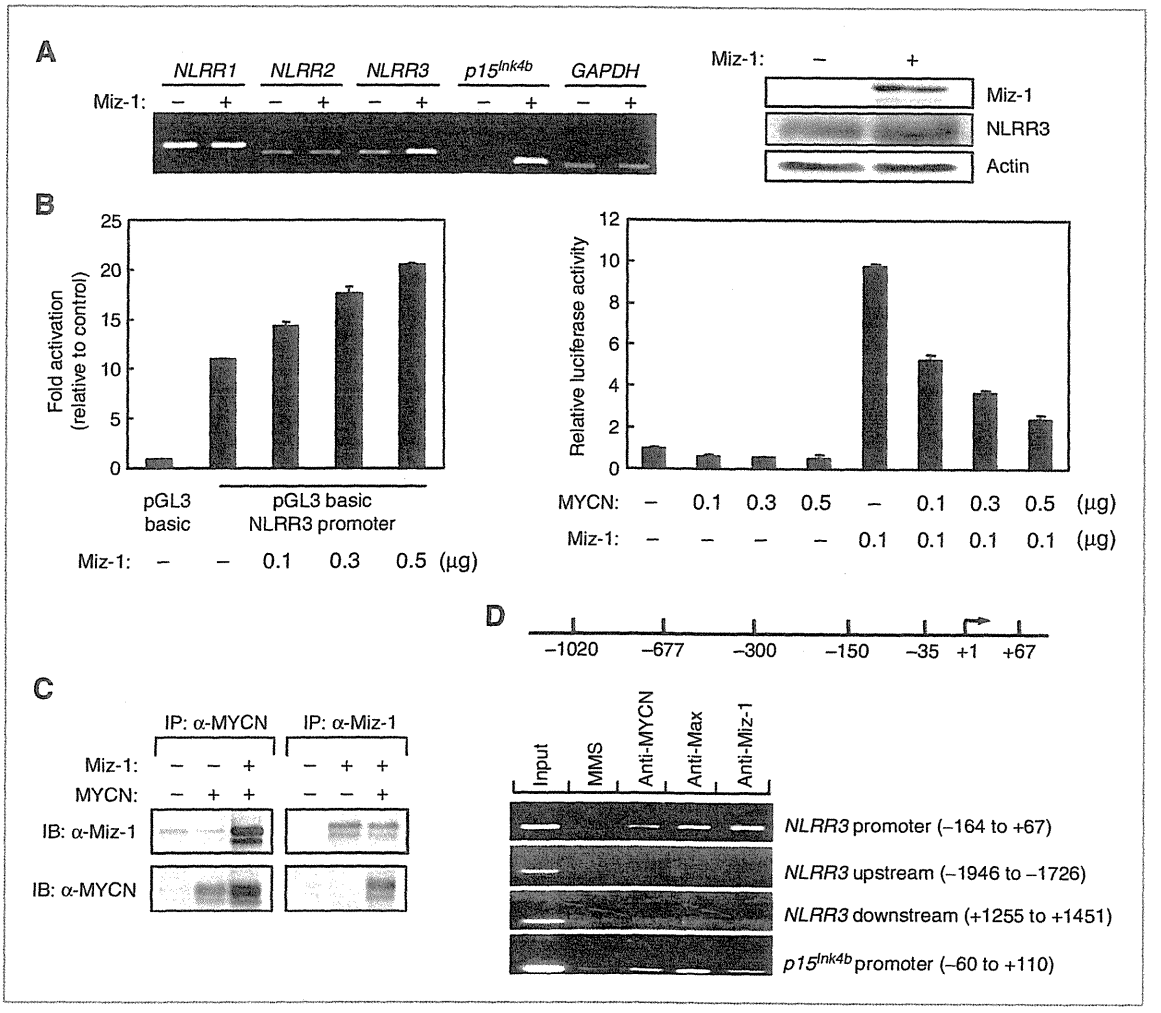

Figure 3. Regulation of the *NLRR3* promoter by MYCN and Miz-1. A, left, RT-PCR analysis showing expression of *NLRR1*, *NLRR2*, *NLRR3*, and $p15^{INk4b}$ in SH-SY5Y cells transiently transfected either with control or Miz-1–expressed plasmid. *GAPDH* was used as an internal control. Right, Western blot showing expression of *NLRR3* and *Miz-1* in SH-SY5Y cells transiently transfected either with control vector or with Miz-1 expressing vector. Actin was used as a loading control. B, left, Miz-1 enhances promoter activity of *NLRR3* in transient transfection assay. Data represent fold activation of the *NLRR3* promoter (−677 to +67) construct upon coexpression of increasing amounts of the expression plasmid for Miz-1 in SY5Y cells. Forty-eight hours after transfection, the cells were lysed and their relative luciferase activities were measured. Firefly luminescence signal was normalized on the basis of *Renilla* luminescence signal. Right, expression of MYCN reduces the basal activity of the *NLRR3* promoter and abrogates transactivation by Miz-1. SH-SY5Y cells were transiently cotransfected with or without constant amount of the expression plasmid for the Miz-1 and 0.1 μg of *NLRR3* promoter (−677 to +67) together with or without the increasing amounts of the expression plasmid for MYCN. The luciferase activity was determined as in B, left. Results are the mean of 3 independent experiments ± SD. C, interaction between MYCN and Miz-1 in NBL cells. Whole cell lysates prepared from SK-N-AS cells transfected with indicated vectors and immunoprecipitated (IP) with the monoclonal anti-MYCN antibody or with polyclonal anti–Miz-1 antibody. The immunoprecipates were analyzed by immunoblotting (IB) with the polyclonal anti–Miz-1 antibody or with monoclonal anti-MYCN antibody, respectively. D, ChIP analysis of SH-SY5Y cells was carried out by using the indicated antibody and PCR primers specific for the different part of *NLRR3* promoter (top 3 panels), upstream, downstream (middle 2 panels) regions of the *NLRR3* gene, and for $p15^{INk4b}$ promoter (bottom).

and *NLRR2*, showed no change. The increased expression of NLRR3 protein was also confirmed by Western blot analysis (Fig. 3A, right). This induction of NLRR3 by Miz-1 was also observed in SK-N-AS cells (Supplementary Fig. S3). To determine whether Miz-1 activates the *NLRR3* promoter, the region spanning exon 2 and 5′-upstream sequences of the *NLRR3* gene (nucleotide −1,020 to +67) was cloned and analyzed for promoter activity by using a luciferase reporter assay. The promoter deletion analysis showed that a nucleotide position between −677 and +67 gives maximum promoter activity (Supplementary Fig. S4A). The core promoter region (−35 to +67) also

Published OnlineFirst September 9, 2011; DOI:10.1158/1078-0432.CCR-11-0313

showed higher promoter activity than other deletion mutants. In transient-cotransfection assays, simultaneous expression of Miz-1 increased the luciferase activities driven by the *NLRR3* promoter (−677 to +67; Fig. 3B, left).

On the contrary, overexpression of MYCN resulted in reduced activity of the *NLRR3* promoter (Supplementary Fig. S4B). These results suggest that Miz-1 and MYCN together contribute to the transcriptional regulation of the *NLRR3* gene. Indeed, the activation of the *NLRR3* promoter by exogenous Miz-1 expression in SH-SY5Y cells was suppressed by coexpression of MYCN in a dose-dependent manner (Fig. 3B, right). The luciferase activities driven by the core promoter region (−35 to +67) also showed a similar result (data not shown). It was reported that a transcriptional suppression of the MYCN-targeted genes occurs when MYCN forms a complex with Miz-1 and Max (19). To make certain of the physical interaction between MYCN and Miz-1, the whole cell lysates prepared from the SK-N-AS cells cotransfected with *MYCN* and *Miz-1* were subjected to an immunoprecipitation assay. As shown in Fig. 3C, coimmunoprecipitation using either MYCN or Miz-1 antibody confirmed that MYCN and Miz-1 formed a complex in SK-N-AS cells as previously reported in non-NBL cell lines (38). Moreover, ChIP analysis revealed that MYCN, Max, and Miz-1 were recruited onto the same promoter region of *NLRR3* (−164 to +67) in SH-SY5Y cells (Fig. 3D). Hence, MYCN negatively regulates *NLRR3* expression by forming a transcriptional complex with Miz-1 in NBL cells.

Increased expression of *NLRR3* and *Miz-1* in favorable neuroblastoma

In our previous report, *NLRR3* is highly expressed in favorable NBLs with a single copy of *MYCN* as compared with NBLs with *MYCN* amplification. To evaluate whether the expression pattern of *Miz-1*, *NLRR3*, and *MYCN* observed in NBL cell lines is consistent in primary NBLs, we analyzed expression levels of those 3 genes in 16 favorable (stages 1 or 2, high expression of *TrkA* and a single copy of *MYCN*) and 16 unfavorable (stages 3 or 4, low expression of TrkA and amplification of *MYCN*) NBL samples by semiquantitative RT-PCR. As shown in Supplementary Fig. S5A, *NLRR3* and *Miz-1* were expressed at higher levels in favorable NBLs than those in unfavorable tumors, whereas the levels of *MYCN* expression were predominantly high in the unfavorable tumors. The expression levels of *NLRR3* and *Miz-1* were also higher in the cell lines with a single copy of *MYCN* than those with *MYCN* amplification, indicating evidence of a positive correlation between *NLRR3* and *Miz-1* expressions and of an inverse correlation between *NLRR3* and *MYCN* expressions (Supplementary Fig. S5B). Those expression patterns were further assessed by immunohistochemistry for NLRR3, MYCN, and Miz-1 in primary NBL tissues (Supplementary Fig. S5C). We carried out immunohistochemical staining on all 11 available paraffin-embedded primary NBL tissues, including 5 NBLs with a single copy of *MYCN* and favorable histology according to INPC (39), 3 NBLs carrying a single copy of *MYCN* with unfavorable histology, and 3 NBLs with *MYCN* amplification and unfavorable histology. As shown in Supplementary Fig. S5C and Supplementary Table S1, the absence of MYCN amplification was associated with strong positive staining of NLRR3 and Miz-1 in all examined samples except one (case 8). All 3 NBLs with *MYCN* amplification showed weak staining for both NLRR3 and Miz-1.

Low expression of *NLRR3* and *Miz-1* is associated with an unfavorable outcome of neuroblastoma

To evaluate whether a statistically significant relationship exists between the patients' survival periods and the expression of *NLRR3*, *Miz-1*, or *MYCN* in primary NBLs, we quantitatively measured the expression levels of *NLRR3*, *Miz-1*, and *MYCN* mRNAs in 87 primary NBLs by using the quantitative real-time PCR method. The clinical features of each NBL samples are listed in Supplementary Table S2. As shown in Table 1, high levels of *NLRR3* expression were significantly associated with younger age ($P = 0.047$), single copy of *MYCN* ($P = 0.047$), favorable disease stages ($P = 0.041$), high levels of *TrkA* expression ($P = 0.042$), and diploid DNA index ($P = 0.003$), but not with tumor origin ($P = 0.933$). A high level of *Miz-1* expression was also significantly associated with younger age ($P = 0.004$), single copy of *MYCN* ($P = 0.004$), favorable disease stages ($P = 0.001$), and high levels of *TrkA* expression ($P = 0.001$), but not with DNA index ($P = 0.060$) and tumor origin ($P = 0.959$). In contrast, a high level of *MYCN* expression was significantly associated with *MYCN* amplification ($P = 0.0001$), advanced disease stages ($P = 0.0031$), low levels of *TrkA* expression ($P = 0.026$), and tumor origin ($P = 0.028$), but not with DNA index ($P = 0.079$), which is consistent with the previous reports (23, 40, 41). There was also a marginal association with patient age ($P = 0.063$). These results suggest that high expression of *NLRR3* and *Miz-1* is well associated with conventional prognostic markers predicting a favorable NBL outcome.

To examine whether the expression levels of *NLRR3*, *Miz-1* and/or *MYCN* have a prognostic significance in primary NBLs, we employed log-rank tests for gene-expression data (Supplementary Table S3). There were significant differences in survival rates in the groups of patients with high and low expression of *NLRR3*, *Miz-1*, and *MYCN*. Patients with high expression of *NLRR3* or *Miz-1* had a higher survival rate than patients with low expression of *NLRR3* or *Miz-1*, and such a difference in survival rate was statistically significant ($P = 0.0023$ and $P = 0.00060$, respectively). However, a patient with high *MYCN* expression was associated with a lower survival rate than that of the *MYCN* low subset ($P < 0.00001$; Supplementary Table S3). Figure 4 shows Kaplan–Meier cumulative survival curves for 87 patients with NBL in terms of expression of *NLRR3*, *Miz-1* and *MYCN*. High expression of *NLRR3* and that of *Miz-1* were significantly associated with good survival ($P = 0.0023$ and $P = 0.00060$, respectively; Fig. 4A, left and right). As already known, high expression of *MYCN*

Published OnlineFirst September 9, 2011; DOI:10.1158/1078-0432.CCR-11-0313

Table 1. Correlation between expression of *NLRR3* or *MYCN* or *Miz-1* and other prognostic factors (Student *t* test)

		NLRR3		*MYCN*		*Miz-1*	
Variable	**No.**	**Mean ± SEM**	***P***	**Mean ± SEM**	***P***	**Mean ± SEM**	***P***
Age, y							
<1	32	0.043 ± 0.011	0.047[a]	0.034 ± 0.013	0.063	0.091 ± 0.019	0.004[a]
≥1	55	0.024 ± 0.003		0.141 ± 0.043		0.042 ± 0.007	
MYCN copy number							
Single copy	58	0.041 ± 0.006	0.047[a]	0.022 ± 0.016	0.0001[a]	0.077 ± 0.012	0.004[a]
Amplified	29	0.019 ± 0.004		0.222 ± 0.053		0.026 ± 0.004	
Tumor stage							
1, 2, 4s	34	0.043 ± 0.009	0.041[a]	0.007 ± 0.002	0.0031[a]	0.093 ± 0.017	0.001[a]
3, 4	53	0.024 ± 0.003		0.144 ± 0.036		0.039 ± 0.007	
TrkA expression							
High	24	0.047 ± 0.013	0.042[a]	0.009 ± 0.003	0.026[a]	0.104 ± 0.024	0.001[a]
Low	61	0.025 ± 0.004		0.125 ± 0.032		0.044 ± 0.006	
DNA index							
Diploidy	42	0.019 ± 0.003	0.003[a]	0.121 ± 0.037	0.079	0.049 ± 0.008	0.06
Aneuploidy	31	0.050 ± 0.010		0.034 ± 0.023		0.085 ± 0.019	
Tumor origin							
Adrenal gland	48	0.032 ± 0.007	0.933	0.135 ± 0.035	0.028[a]	0.059 ± 0.012	0.959
Others	39	0.032 ± 0.004		0.034 ± 0.025		0.060 ± 0.011	

[a]$P < 0.05$.

was strongly associated with a poor prognosis of NBL ($P < 0.00001$; Fig. 4A, middle). Remarkably, the combination of low levels of both *NLRR3* and *Miz-1* expressions showed a significantly worse prognosis as compared with the other combination, high *NLRR3* and *Miz-1* expressions ($P = 0.0012$; Fig. 4C). Furthermore, the combination of low expression of *NLRR3* and high expression of *MYCN* showed a significantly worse prognosis than the combination of high expression of *NLRR3* and low expression of *MYCN* ($P < 0.00001$; Fig. 4B). In NBLs with low expression of *MYCN*, the expression levels of *NLRR3* could segregate the prognosis into good and intermediate groups.

The univariate Cox regression analysis shown in Table 2 was employed to examine the individual relationship of each variable to survival. The results in Table 2 showed that *NLRR3* expression, *MYCN* expression, *Miz-1* expression, age, *MYCN* amplification, stage *TrkA* expression, and origin were of prognostic importance, supporting the results of the log-rank test. Moreover, the multivariate Cox models were fitted to assess the predictive importance of NLRR3 expression for survival after controlling other prognostic factors. The results in Table 2 showed that *NLRR3* expression was significantly associated with survival after controlling *TrkA* expression ($P = 0.0212$), suggesting that *NLRR3* expression was an independent prognostic factor from *TrkA* expression (Table 2). This suggests that *NLRR3* expression is associated with survival after controlling *MYCN* expression ($P = 0.0610$), *Miz-1* expression ($P = 0.1510$), *MYCN* amplification ($P = 0.1210$), and stage ($P = 0.1040$), and also supports that *NLRR3* expression could serve as a prognostic biomarker for NBL tumors dependent on both MYCN and Miz-1 expression as well as *MYCN* amplification.

Discussion

In primary human NBLs, *MYCN* is frequently amplified and thereby one of the most important prognostic factors. In this study, we found that *NLRR3* is a direct target of MYCN but its expression is negatively regulated by MYCN in association with Miz-1. In primary NBLs, both *NLRR3* and *Miz-1* are expressed at significantly high levels in favorable NBLs and downregulated in *MYCN*-amplified aggressive tumors.

In general, favorable NBL cells show more differentiated features than unfavorable cells (30). The treatment of NBL cells with ATRA induces neuronal differentiation accompanied with growth inhibition and reduction of *MYCN* expression (33). Under such conditions, *NLRR3* is induced while *MYCN* is decreased (Figs. 1 and 2). These results suggest a functional inverse relationship between MYCN and NLRR3 in cellular differentiation and tumor development. In some NBL cell lines, siRNA-mediated knockdown of endogenous MYCN caused NLRR3 induction; conversely, ectopic expression of MYCN resulted in a decreased expression of *NLRR3*. Hence, the inverse regulatory relationship between NLRR3 and MYCN may be present as a

Published OnlineFirst September 9, 2011; DOI:10.1158/1078-0432.CCR-11-0313

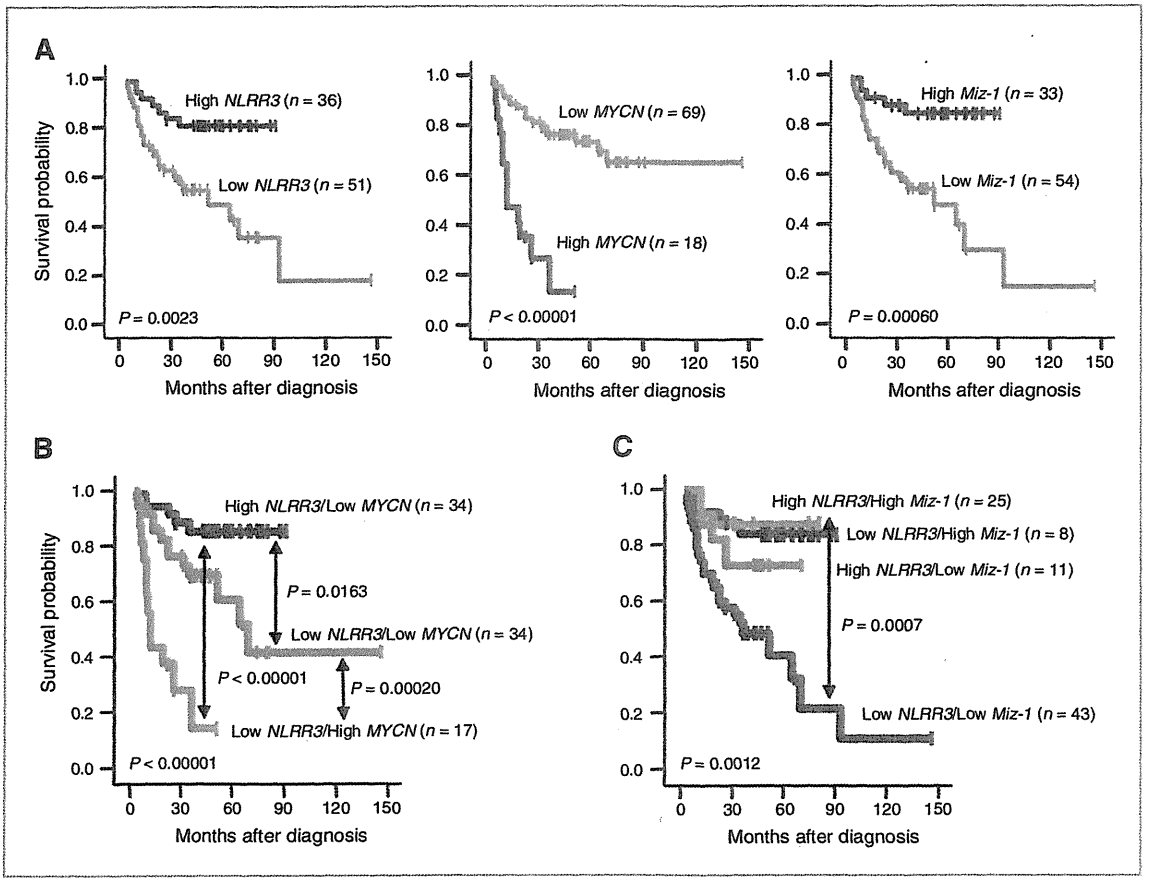

Figure 4. Real-time PCR analysis for the expression of *NLRR3*, *MYCN*, and *Miz-1* in 87 primary NBLs. Kaplan–Meier survival curves of patients with NBLs on the basis of higher or lower expression levels of *NLRR3* (A, left); *MYCN* (A, middle); *Miz-1* (A, right); *NLRR3* and *MYCN* (B); or *NLRR3* and *Miz-1* (C). In case of *NLRR3* and *MYCN* survival curve, high NLRR3/high MYCN group was excluded because this group consists of only 2 samples. Relative expression levels of *NLRR3* or *MYCN* or *Miz-1* mRNA were determined by calculating the ratio between *GAPDH* and *NLRR3* or *MYCN* or *Miz-1*.

consequence of MYCN-induced transcriptional downregulation of *NLRR3*.

MYCN protein is an important regulator of many cellular processes, including growth, proliferation, differentiation, and apoptosis (42). A part of these diverse cellular functions of MYCN may be due to the combined abilities of both activating and repressing transcription of the target genes (42). Transcriptional activation by MYCN occurs *via* dimerization with its partner protein, Max, and direct binding to specific DNA sequences named E-boxes. MYCN directly binds and stimulates the expression of approximately 4,000 of the E-box containing genes (43). Although heterodimerization of Max with MYCN is necessary to regulate gene expression, the other proteins including *Miz-1* may bind to C-terminal MYCN in addition to Max (19, 20, 44). Concurrent binding of these factors redirects the MYCN/Max dimer to noncanonical sites such as the initiator element, where this complex might prevent the efficient binding of basal transcriptional machinery or coactivators necessary for transactivation, resulting in repression of gene expression (38, 44). The dimerization with MYCN switches Miz-1 from a transcriptional activator to a repressor of the target genes, likely by preventing the interaction of Miz-1 with its own coactivator (19, 20). Several studies have shown that Miz-1 binds and activates the promoter of several genes, including $p15^{INK4b}$ and $p21^{CIP1}$, and the transactivation can be negatively regulated by its association with MYCN (16, 17, 29). Regarding the reduction of NLRR3 expression observed in this study, Miz-1 seems to be a key molecule forming a transcription factor complex with MYCN. Because Miz-1 itself acts as an activator of *NLRR3* promoter, *NLRR3* expression may be switched on and off through Miz-1 in the absence and presence of MYCN, respectively. Although the expression levels of Miz-1 in unfavorable NBLs are relatively low, its amount still may be enough to act with MYCN to inhibit transactivation of *NLRR3* in NBLs.

Published OnlineFirst September 9, 2011; DOI:10.1158/1078-0432.CCR-11-0313

Table 2. Multiple Cox regression model using NLRR3 expression and dichotomous factors of MYCN expression, Miz-1 expression, age, MYCN amplification, stage, TrkA expression, and origin ($n = 87$)

Model	Factor	*P*	HR (95% CI)
Univariate analysis			
A	*NLRR3* mRNA expression (high vs. low)	0.0041[a]	0.291 (0.125–0.678)
B	*MYCN mRNA* expression (high vs. low)	<0.0001[a]	5.050 (2.450–10.40)
C	*Miz-1* mRNA expression (high vs. low)	0.0021[a]	0.212 (0.080–0.561)
D	Age (≥1 vs. <1 y)	0.0161[a]	0.309 (0.119–0.803)
E	*MYCN* amplification (single copy vs. amplified)	<0.0001[a]	4.628 (2.281–9.387)
F	Stage (1,2,4s vs. 3,4)	0.0010[a]	12.66 (3.023–53.09)
G	*TrkA* expression (high vs. low)	0.0070[a]	7.180 (1.714–30.07)
H	Origin (adrenal gland vs. others)	0.0480[a]	2.125 (1.005–4.491)
Multivariate analysis			
A	*NLRR3* mRNA expression (high vs. low)	0.061	0.424 (0.172–1.041)
	MYCN mRNA expression (high vs. low)	0.0011[a]	3.707 (1.735–7.921)
B	*NLRR3* mRNA expression (high vs. low)	0.151	0.503 (0.198–1.283)
	Miz-1 mRNA expression (high vs. low)	0.0301[a]	0.304 (0.104–0.893)
C	*NLRR3* mRNA expression (high vs. low)	0.0150[a]	0.347 (0.148–0.814)
	Age (≥1 vs. <1 y)	0.053	0.384 (0.146–1.013)
D	*NLRR3* mRNA expression (high vs. low)	0.121	0.545 (0.253–1.173)
	MYCN amplification (single copy vs. amplified)	0.0001[a]	3.940 (1.893–8.203)
E	*NLRR3* mRNA expression (high vs. low)	0.104	0.493 (0.210–1.156)
	Stage (1, 2, 4s vs. 3, 4)	0.0020[a]	10.108 (2.359–43.309)
F	*NLRR3* mRNA expression (high vs. low)	0.0212[a]	0.361 (0.152–0.863)
	TrkA expression (high vs. low)	0.0163[a]	5.892 (1.395–24.901)
G	*NLRR3* mRNA expression (high vs. low)	0.0070[a]	0.308 (0.132–0.720)
	Origin (adrenal gland vs. others)	0.084	1.937 (0.914–4.104)

NOTE: All variables with 2 categories. HR shows the relative risk of death of first category relative to the second.
[a]$P < 0.05$.

Inhibition of cellular differentiation is one of the well-known biological functions of MYCN. Because differentiated NBL cells have a high expression of NLRR3 instead of MYCN, the reduced expression of NLRR3 in undifferentiated, unfavorable NBL cells may propose an important component of the mechanism by which MYCN functions against cell differentiation. As ectopic expression of NLRR3 induced morphologic changes indicative of neuronal differentiation accompanying with neurite outgrowth (data not shown), the downregulation of NLRR3 by MYCN might contribute to the well-documented stimulation of cell proliferation by MYCN. Although there are MYCN target genes that are potentially involved in cell-cycle progression, including *α-prothymosin, ornithine decarboxylase, MCM7, ID2, MDM2,* and *NLRR1* (27, 36, 45–47), suppression of NLRR3 might have an additive effect on NBL cell proliferation. Our log-rank test showed that expression of NLRR3 is well associated with a favorable prognosis, suggesting its involvement in NBL differentiation. Of more interest, NLRR3 and NLRR1 seem to function oppositely in NBL. Thus, the expression of NLRR3 is a new prognostic indicator of NBL and may be involved in regulating the biology of the tumor.

Collectively, our present findings suggest that the repression of NLRR3 mediated by MYCN requires an association with Miz-1 and also contributes to the favorable outcome of NBLs. The expression pattern of NLRR3, Miz-1, and MYCN might play an important role in defining the clinical behavior of NBLs. Because NLRR3 is an orphan receptor, the future discovery of its ligand(s) may unveil the molecular mechanism of tumorigenesis, differentiation, and proliferation of NBL. Further investigation is necessary to clarify whether NLRR3 is an important primary cue for developing novel diagnostic and therapeutic strategies against high-risk NBLs.

Disclosure of Potential Conflicts of interest

No potential conflicts of interest were disclosed.

Acknowledgments

The authors thank Drs. Y. Nakamura and E. Isogai (Chiba Cancer Center Research Institute, Chiba, Japan) for their outstanding technical assistance, and Dr. Hiroki Nagase (Chiba Cancer Center Research Institute, Chiba, Japan) and Ms. Paula D. Jones (Roswell Park Cancer Institute, Buffalo, NY) for critical reading of the article.

Published OnlineFirst September 9, 2011; DOI:10.1158/1078-0432.CCR-11-0313

Grant Support

This work was supported in part by a grant-in-aid from the Ministry of Health, Labour and Welfare for Third Term Comprehensive Control Research for Cancer (A. Nakagawara), a grant-in-aid for Scientific Research on Priority Areas from the Ministry of Education, Culture, Sports, Science and Technology, Japan (A. Nakagawara), and a grant-in-aid for Scientific Research from the Japanese Society for the Promotion of Science (A. Takatori and A. Nakagawara).

The costs of publication of this article were defrayed in part by the payment of page charges. This article must therefore be hereby marked *advertisement* in accordance with 18 U.S.C. Section 1734 solely to indicate this fact.

Received February 3, 2011; revised August 3, 2011; accepted August 9, 2011; published OnlineFirst September 9, 2011.

References

1. Westemann F, Schwab M. Genetic parameters of neuroblastomas. Cancer Lett 2002;184:127–47.
2. Brodeur GM, Nakagawara A. Molecular basis of clinical heterogeneity in neuroblastoma. Am J Pediatr Hematol Oncol 1992;14: 111–6.
3. Nakagawara A, Arima M, Azar CG, Scavarda NJ, Brodeur GM. Inverse relationship between trk expression and N-myc amplification in human neuroblastomas. Cancer Res 1992;52:1364–68.
4. Nakagawara A, Arima-Nakagwara M, Scavarda NJ, Azar CG, Cantor AB, Brodeur GM. Association between high levels of expression of the TRK gene and favorable outcome in human neuroblastoma. New Engl J Med 1993;328:847–54.
5. Nakagawara A, Azar CG, Scavarda NJ, Brodeur GM. Expression and function of TRK-B and BDNF in human neuroblastomas. Mol Cell Biol 1994;14:759–67.
6. Nakagawara A, Arima-Nakagawara M, Azar CG, Scavarda NJ, Brodeur GM. Clinical significance of expression of neurotrophic factors and their receptors in neuroblastoma. Prog Clin Biol Res 1994;385: 155–61.
7. Seeger RC, Brodeur GM, Sather H, Dalton A, Siegel SE, Wong KY, et al. Associations of multiple copies of the N-myc oncogene with rapid progression of neuroblastomas. New Engl J Med 1985;313: 1111–6.
8. Kohl NE, Gee CE, Alt FW. Activated expression of the N-myc gene in human neuroblastomas and related tumors. Science 1984;226: 1335–7.
9. Nisen PD, Waber PG, Rich MA, Pierce S, Garvin JR, Gilbert F, et al. N-myc oncogene RNA expression in neuroblastoma. J Natl Cancer Inst 1988;80:1633–7.
10. Slavc I, Ellenbogen R, Jung WH, Vawter GF, Kretschmar C, Grier H, et al. Myc gene amplification and expression in primary human neuroblastoma. Cancer Res 1990;50:1459–63.
11. Seeger RC, Wada R, Brodeur GM, Moss TJ, Bjork RL, Sousa L, et al. Expression of N-myc by neuroblastomas with one or multiple copies of the oncogene. Prog Clin Biol Res 1988;271:41–9.
12. Schwab M, Ellison J, Busch M, Rosenau W, Varmus HE, Bishop JM. Enhanced expression of the human gene N-myc consequent to amplification of DNA may contribute to malignant progression of neuroblastoma. Proc Natl Acad Sci U S A 1984;81:4940–4.
13. Cohn SL, Tweddle DA. MYCN amplification remains prognostically strong 20 years after its "clinical debut". Eur J Cancer 2004;40: 2639–42.
14. Strieder V, Lutz W. Regulation of N-myc expression in development and diseases. Cancer Lett 2002;180:107–19.
15. Kouzarides T, Ziff E. The role of the leucine zipper in the fos-jun interaction. Nature 1988;336:646–51.
16. Landschulz WH, Johnson PF, Mcknight SL. The leucine zipper: a hypothetical structure common to a new class of DNA binding proteins. Science 1988;240:1759–64.
17. Alex R, Sozeri O, Meyer S, Dildrop R. Determination of the DNA sequence recognized by the bHLH-zip domain of the N-Myc protein. Nucleic Acids Res 1992;20:2257–63.
18. Blackwood EM, Kretzner L, Eisenman RN. Myc and Max function as a nucleoprotein complex. Curr Opin Genet Dev 1992;2:227–35.
19. Staller P, Peukert K, Kiermaier A, Seoane J, Lukas J, Karsunky H, et al. Repression of p15INK4b expression by Myc through association with Miz-1. Nature Cell Biol 2001;3:392–9.
20. Wu S, Cetinkaya C, Munoz-Alonso MJ, Von der Lehr N, Bahram F, Beuger V, et al. Myc represses differentiation-induced p21CIP1 expression via Miz-1-dependent interaction with the p21 core promoter. Oncogene 2003;22:351–60.
21. Zhang J, Li F, Liu X, Shen L, Liu J, Su J, et al. The repression of human differentiated-related gene NDRG2 expression by Myc via Miz-1 dependent interaction with the NDRG2 core promoter. J Biol Chem 2006;281:39159–68.
22. Koppen A, Ait-Aissa R, Hopman S, Koster J, Haneveld F, Versteeg R, et al. Dickkopf-1 is down-regulated by MYCN and inhibits neuroblastoma cell proliferation. Cancer Lett 2007;256:218–28.
23. Hamano S, Ohira M, Isogai E, Nakada K, Nakagawara A. Identification of novel human neuronal leucine-rich repeat (hNLRR) family genes and inverse association of expression of Nbla10449/hNLRR-1 and Nbla10677/hNLRR-3 with the prognosis of primary neuroblastomas. Int J Oncol 2004;24:1457–66.
24. Ohira M, Morohashi A, Inuzuka H, Shishikura T, Kawamoto T, Kageyama H, et al. Expression profiling and characterization of 4200 genes cloned from primary neuroblastomas: identification of 305 genes differentially expressed between favorable and unfavorable subsets. Oncogene 2003;22:5525–36.
25. Hayata T, Uochi T, Asashima M. Molecular cloning of XNLRR-1, a Xenopus homolog of mouse neuronal leucine-rich repeat protein expressed in the developing Xenopus nervous system. Gene 1998;221:159–66.
26. Fukamachi K, Matsuoka Y, Ohno H, Hamaguchi T, Tsuda H. Neuronal leucine-rich repeat protein-3 amplifies MAPK activation by epidermal growth factor through a carboxyl-terminal region containing endocytosis motifs. J Biol Chem 2002;277:43549–52.
27. Hossain MS, Ozaki T, Wang H, Nakagawa A, Takenobu H, Ohira M, et al. N-MYC promotes cell proliferation through a direct transactivation of neuronal leucine-rich repeat protein-1 (NLRR1) gene in neuroblastoma. Oncogene 2008;27:6075–82.
28. Ishii N, Wanaka A, Tohyama M. Increased expression of NLRR-3 mRNA after cortical brain injury in mouse. Molecular Brain Research 1996;40:148–52.
29. Brodeur GM, Pritchard J, Berthold F, Carlsen NL, Castel V, Castelberry RP, et al. Revisions of the international criteria for neuroblastoma. Diagnosis, staging, and response to treatment. J Clin Oncol 1993;11:1466–77.
30. Matsumura T, Iehara T, Sawada T, Tsuchida Y. Prospective study for establishing the optimal therapy of infantile neuroblastoma in Japan. Med Pediatr Oncol 1998;31:210.
31. Kaneko M, Nishihira H, Mugishima H, Ohnuma N, Nakada K, Kawa K, et al. Stratification of treatment of stage 4 neuroblastoma patients based on N-myc amplification status. Study Group of Japan for Treatment of Advanced Neuroblastoma, Tokyo, Japan. Med Pediatr Oncol 1998;31:1–7.
32. Melino G, Thiele CJ, Knight RA, Piacentini M. Retinoids and the control of growth/death decisions in human neuroblastoma cell lines. J Neurooncol 1997;31:65–83.
33. Thiele CJ, Reynolds CP, Israel MA. Decreased expression of N-myc precedes retinoic acid-induced morphological differentiation of human neuroblastoma. Nature 1985;313:404–6.
34. Niizuma H, Nakamura Y, Ozaki T, Nakanishi H, Ohira M, Isogai E, et al. Bcl-2 is a key regulator for the retinoic acid-induced apoptopic cell death in neuroblastoma. Oncogene 2006;25:5046–55.
35. Bjelfman C, Meyerson G, Cartwright CA, Mellstrom K, Hammerling U, Pahlman S. Early activation of endogenous pp60src kinase activity during neuronal differentiation of cultured human neuroblastoma cells. Mol Cell Biol 1990;10:361–70.

Published OnlineFirst September 9, 2011; DOI:10.1158/1078-0432.CCR-11-0313

36. Lutz W, Stohr M, Schurmann J, Wenzel A, Lohr A,Schwab M. Conditional expression of N-myc in human neuroblastoma cells increases expression of α-prothymosin and ornithine decarboxylase and accelerates progression into S-phase after mitogenic stimulation of quiescent cells. Oncogene 1996;13:803–12.
37. Chen L, Peng Z, Bateman E. In vivo interactions of the Acanthamoeba TBP gene promoter. Nucleic acids Res 2004;32: 1251–60.
38. Peukert K, Staller P, Schneider A, Carmichael G, Hanel F,Eilers M. An alternative pathway for gene regulation by Myc. EMBO J 1997;16: 5672–86.
39. Shimada H, Ambros IM, Dehner LP, Hata J, Joshi VV, Roald B, et al. The International Neuroblastoma Pathology Classification (the Shimada System). Cancer 1999;86: 364–72.
40. Ikegaki N, Gotoh T, Kung B, Riceberg JS, Kim DY, Zhao H, et al. De novo identification of MIZ-1 (ZBTB17) encoding a MYC-interacting zinc-finger protein as a new favorable neuroblastoma gene. Clin Cancer Res 2007;13:6001–9.
41. Tang XX, Zhou H, Kung B, Kim DY, Hicks SL, Cohn SL, et al. The MYCN enigma: significance of MYCN expression in neuroblastoma. Cancer Res 2006;66:2826–33.
42. Pelengaris S, Khan M, Evan G. c-MYC: more than just a matter of life and death. Nat Rev Cancer 2002;2:764–76.
43. Levens DL. Reconstructing MYC. Genes dev 2003;17:1071–7.
44. Wanzel M, Herold S, Eilers M. Transcriptional repression by Myc. Trends Cell Biol 2003;13:146–50.
45. Shohet JM, Hicks MJ, Plon SE, Burlingame SM, Stuart S, Chen SY, et al. Minichromosome maintenance protein MCM7 is a direct target of the MYCN transcription factor in neuroblastoma. Cancer Res 2002;62:1123–8.
46. Iasorella A, Noseda M, Beyna M, Yokota Y, Iavarone A. Id2 is a retinoblastoma protein target and mediates signaling by Myc oncoproteins. Nature 2000;407:592–8.
47. Slack A, Chen Z, Tonelli R, Pule M, Hunt L, Pession A, et al. The p53 regulatory gene MDM2 is a direct transcriptional target of MYCN in neuroblastoma. Proc Natl Acad Sci U S A 2005;102:731–6.

MOLECULAR AND CELLULAR BIOLOGY, Jan. 2011, p. 351–364 Vol. 31, No. 2
0270-7306/11/$12.00 doi:10.1128/MCB.00259-10

Mammalian Polycomb-Like Pcl2/Mtf2 Is a Novel Regulatory Component of PRC2 That Can Differentially Modulate Polycomb Activity both at the *Hox* Gene Cluster and at *Cdkn2a* Genes▽

Xiangzhi Li,[1] Kyo-ichi Isono,[1]† Daisuke Yamada,[1]† Takaho A. Endo,[2] Mitsuhiro Endoh,[1,3] Jun Shinga,[1] Yoko Mizutani-Koseki,[1] Arie P. Otte,[4] Miguel Casanova,[5] Hiroshi Kitamura,[1] Takehiko Kamijo,[6] Jafar Sharif,[1] Osamu Ohara,[1] Tetsuro Toyada,[2] Bradley E. Bernstein,[7] Neil Brockdorff,[5] and Haruhiko Koseki[1,3]*

RIKEN Research Center for Allergy and Immunology[1] and RIKEN Bioinformatics and Systems Engineering Division,[2] 1-7-22 Suehiro, Tsurumi-ku, Yokohama 230-0045, Japan; JST, CREST, 1-7-22 Suehiro, Tsurumi-ku, Yokohama 230-0045, Japan[3]; Swammerdam Institute for Life Sciences, University of Amsterdam, Kruislaan 406, 1098 SM Amsterdam, Netherlands[4]; Department of Biochemistry, University of Oxford, South Parks Road, Oxford OX1 3QU, United Kingdom[5]; Division of Biochemistry, Chiba Cancer Center Research Institute, 666-2 Nitona, Chuoh-ku, Chiba 260-8717, Japan[6]; and MGH Pathology, Harvard University, 185 Cambridge Street, Boston, Massachusetts 02114[7]

Received 8 March 2010/Returned for modification 17 April 2010/Accepted 23 October 2010

The Polycomb group of proteins forms at least two distinct complexes designated the Polycomb repressive complex-1 (PRC1) and PRC2. These complexes cooperate to mediate transcriptional repression of their target genes, including the *Hox* gene cluster and the *Cdkn2a* genes. Mammalian Polycomb-like gene Pcl2/Mtf2 is expressed as four different isoforms, and the longest one contains a Tudor domain and two plant homeodomain (PHD) fingers. Pcl2 forms a complex with PRC2 and binds to *Hox* genes in a PRC2-dependent manner. We show that Pcl2 is a functional component of PRC2 and is required for PRC2-mediated *Hox* repression. Pcl2, however, exhibits a profound synergistic effect on PRC1-mediated *Hox* repression, which is not accompanied by major alterations in the local trimethylation of histone H3 at lysine 27 (H3K27me3) or PRC1 deposition. Pcl2 therefore functions in collaboration with both PRC2 and PRC1 to repress *Hox* gene expression during axial development. Paradoxically, in embryonic fibroblasts, Pcl2 is shown to activate the expression of *Cdkn2a* and promote cellular senescence, presumably by suppressing the catalytic activity of PRC2 locally. Taken together, we show that Pcl2 differentially regulates Polycomb-mediated repression of *Hox* and *Cdkn2a* genes. We therefore propose a novel role for Pcl2 to modify functional engagement of PRC2 and PRC1, which could be modulated by sensing cellular circumstances.

The Polycomb group (PcG) was first identified in *Drosophila melanogaster* as a gene cluster necessary for the maintenance of segmental identity (50, 53). The PcG proteins are required for the epigenetic repression of a number of developmental regulatory genes, including homeotic genes. They do so by forming at least two distinct multimeric protein complexes at their target loci, known as Polycomb repressive complex-1 (PRC1) and PRC2 (11, 13, 46, 57).

In *Drosophila*, the core PRC1 is formed by four proteins, Polycomb (Pc), Polyhomeotic (Ph), Posterior sex combs (Psc), and dRing (Sex comb extra; Sce), which inhibit the chromatin remodeling activity of SWI/SNF complexes (20, 35). Mammalian orthologs form functionally similar complexes (40). PRC1 has been shown to act as an E3 component for ubiquitination of histone H2A at lysine 119 (uH2A) via Ring1B and Ring1A catalytic subunits (9, 14, 62). In addition, regulation of higher-order chromatin structure is a recently identified function mediated by PRC1 (19). The core of the mammalian PRC2 is composed of three evolutionarily conserved proteins, Eed, an ortholog of extra sex combs [Esc]), Ezh2, an ortholog of enhancer of zeste [E(z)], and Suz12, which mediates trimethylation of histone H3 at lysine 27 by the Ezh2 component (11, 13, 46, 48, 51, 60). Although both PRC1 and PRC2 are required to maintain *Hox* repression and share target loci in both vertebrates and invertebrates, these complexes do not associate with each other in most cell types. A plausible model for Polycomb silencing is through the engagement of PRC1 with the target via its interaction with H3K27me3 mediated by the chromodomain of Pc or its mammalian counterparts (11, 62). However, recent genome-wide analysis of PRC1 and PRC2 occupancy revealed that PRC1 binding demarcated a portion of the PRC2 targets (37), implying that functional engagement of PRC1 and PRC2 is not constitutive but, instead, is regulated by undefined intrinsic and/or extrinsic signals.

The *polycomblike* (*Pcl*) gene was initially isolated as a PcG gene during a *Pc* mutation modifier screen in *D. melanogaster* and then identified in several studies as an enhancer

* Corresponding author. Mailing address: RIKEN Research Center for Allergy and Immunology, 1-7-22 Suehiro, Tsurumi-ku, Yokohama 230-0045, Japan. Phone: 81 45 503 9689. Fax: 81 45 503 9688. E-mail: koseki@rcai.riken.jp.
† K.-I.I. and D.Y. contributed equally to this work.
▽ Published ahead of print on 8 November 2010.

TABLE 1. Antibodies used in this study

Specificity	Species	Antibody type	Source or reference	Catalog or clone no.
Pcl2	Mouse	Monoclonal	This paper	3A9
Pcl2	Rabbit	Antiserum	This paper	
Rnf2	Mouse	Monoclonal	5	Clone 3
Phc2	Mouse	Monoclonal	28	4G9
Mel18	Goat	Antiserum	Santa Cruz (Santa Cruz, CA)	C-20
Mel18	Rabbit	Antiserum	Santa Cruz (Santa Cruz, CA)	H-115
Eed	Mouse	Monoclonal	23	M26
Ezh2	Mouse	Monoclonal	23	M10
Ezh2	Rabbit	Monoclonal	Upstate (Lake Placid, NY)	07-400
Suz12	Rabbit	Antiserum	Upstate (Lake Placid, NY)	07-379
Histone H3K27me3	Rabbit	Antiserum	Upstate (Lake Placid, NY)	07-449
Histone H3K4me3	Rabbit	Antiserum	Upstate (Lake Placid, NY)	07-473
Histone H2Aub1	Mouse	Monoclonal	Upstate (Lake Placid, NY,)	E6C5
FLAG	Mouse	Monoclonal	Sigma-Aldrich (St. Louis, MO)	F-3165
Myc	Mouse	Monoclonal	Upstate (Lake Placid, NY)	4A6
γ-Tubulin	Rabbit	Antiserum	Sigma-Aldrich (St. Louis, MO)	T3320
$p19^{ARF}$	Rabbit	Antiserum	Abcam (Cambridge, UK)	R562
$p16^{ink4a}$	Rat	Monoclonal	NeoMarkers (Fremont, CA)	16P04

for *Esc* mutations (17, 33). *Pcl* mutant phenotypes are similar to those of *Pc* mutants, and interactions between mutant *Pcl* and *Pc* or *Esc* synergistically enhance the respective phenotypes in a dose-dependent manner. The Pcl protein has a Tudor domain and two tandem plant homeodomain (PHD) fingers (43, 49, 64). Pcl has been shown to be a part of two distinct protein complexes, PRC2 and a thus far uncharacterized complex, which appear at *Drosophila* embryonic and larval stages, respectively (47, 56, 61). In *Drosophila* embryos, Pcl forms complexes with PRC2 and maximizes its catalytic activity at Polycomb target genes (47). In the larval stage, although Pcl does not form complexes with PRC2, it mediates pleiohomeotic-dependent PRC2 target binding (56). These findings imply that Pcl plays at least two distinct roles in regulating the expression of Polycomb targets by interacting with different protein complexes and suggest that these interactions depend on the developmental stage or cell type. The picture may be even more complex because functional interactions of Pcl could potentially extend to PRC1. In addition, Pcl has been shown to display extensive colocalization with Pc and Polyhomeotic (Ph) proteins on the polytene chromosomes (43), and genetic interactions between *Pcl* and *Pc* have also been demonstrated (33). These observations suggest that Pcl may have multiple regulatory functions in mediating Polycomb repression.

Three homologs of the *Drosophila Pcl* gene have been identified in vertebrates, frogs, chickens, and mammals and are named, *Pcl1* (also *Phf1* or *tctex3*), *Pcl2/Mtf2* (also *M96*; here, designated *Pcl2*) and *Pcl3* (also *Phf19*) (12, 27, 32, 36, 64, 66). Overexpression studies using *Xenopus* and chicken embryos demonstrated that Pcl1 and/or Pcl2 mediates the repression of developmental regulatory genes such as *En-2*, *Krox20*, *Hoxb9*, and *Shh* (36, 64, 66). Murine and human orthologs of these genes have been shown to be the targets of PRC1 and PRC2 as revealed by genome-wide chromatin immunoprecipitation (ChIP) assays (8, 38). These findings imply that vertebrate as well as *Drosophila* Pcl family proteins may be part of the PcG complex. In support of this idea, hPHF1 was copurified with a subset of PRC2 and was shown to enhance the catalytic activity of PRC2 in a human cell line (10, 55). Unexpectedly, however, hPHF1 was also found to form complexes with proteins involved in the DNA damage response (25). Despite these recent advances, the molecular basis underlying the multiple functions of Pcl family proteins is not well understood. Although the biochemical properties of hPHF1 have been elucidated, a genetic approach using loss-of-function mutants of the mammalian *Pcl* family is still needed to clarify the genetic cascades involving the Pcl orthologs. A study using a *Pcl2* gene trap allele suggested the involvement of Pcl2 in anterior-posterior (A-P) specification of the axis (63); however, the mechanistic basis of the involvement remains unclear. To address these questions, we have combined genetic and biochemical approaches to clarify the role of Pcl2 in Polycomb-mediated repression at the *Hox* gene cluster and *Cdkn2a* genes.

MATERIALS AND METHODS

Determination of *Pcl2* gene structure. Data sets of RNA-Seq experiments performed by Motazavi et al. (45) were downloaded (http://woldlab.caltech.edu/~alim/RNAseq/). Results from two biological replicates were summed for three cell types (brain, liver, and muscle). Positions of the 15 *Pcl2* exons (*Mtf2* in the database) were identified using the BLASTN (3) program with *Mtf2* as the reference sequence (GenBank accession number NM_013827.2) and mouse chromosome 5 (NCBI version 37) (see Fig. S1A posted at http://web.rcai.riken.jp/en/paper_figs/Li_Supp_figs_rev3.pdf).

Production of anti-Pcl2 monoclonal antibody (MAb) and antiserum. A partial cDNA fragment that included the PHD fingers (amino acids [aa] 103 tp 327) of Pcl2 was isolated by yeast two-hybrid screening for Mel18-interacters and subcloned into the pGEX-4T-3 vector (Amersham Biosciences) to express a glutathione *S*-transferase (GST)-Pcl2 fusion protein. This fusion protein was used to generate hybridomas as described previously (29). Rabbit polyclonal antiserum was raised against a synthetic polypeptide corresponding to amino acids 20 to 36 of Pcl2 (RNQKTSASLNKLSLQDGC) conjugated to keyhole limpet hemocyanin. A purified IgG fraction of this antiserum was used for immunoprecipitation (IP) and immunofluorescence.

Immunoprecipitation, Western blot analyses, and gel filtration chromatography. IP and Western blot analyses were performed as described previously (28). Antibodies used in this study are listed in Table 1 (5, 23, 28). Nuclear proteins were extracted from nuclear pellets of K562 cells as described previously (15). Nuclear extracts were loaded onto Superose 6 columns (Amersham Biosciences), and 0.5-ml fractions were collected. Proteins from each fraction were concentrated by trichloroacetic acid-deoxycholate precipita-

TABLE 2. PCR primers used in this study

Primer function	Name	Primer sequence	
		Forward	Reverse
ChIP	Hoxa4	AGCTCCAGCCCTGGCTTCGC	CGTGATGGATGCTGCTAGCC
	Hoxb4	AAACCGAGTCAAGGGGTCGG	CGCGTAGCGCTGCACAGTGC
	Hoxb6	CCGCATAGCCAGACGAGTAG	CTGCCTCTGCCATTGGTCAG
	Hoxb8	TGGAGCTGGAGAAGGAGTTCCTA	CAGAAGCTATTACGAGATACTACC
	Hprt	CTCCTAAGGTTACTAAGTAG	CAAAGGCAGTTCCGGAACTC
	Ink4a	CTACAGAAGAGATGCAGGGTTC	AAGGAGAGATTTCGAGAAGGAC
	Actin	CTACACGCTAGGCGTAAAGTTG	TCTCGTGGCTAGTACCTCACTG
RT-PCR	Hoxa1	AGATGGACAATGCAAGAATG	TCAGTGGGAGGTAGTCAGAG
	Hoxb3	ACCTACTACGACAACACCGC	TGCGACGGTTCTGGAACCAG
	Hoxb4	GATCAACTCAAACTATGTCG	TGGTGTTGGGCAACTTGTGG
	Hoxb6	GTTCCTATTTCGTGAACTCC	AGCACCTTCACTCGGCTGGC
	Hoxb8	GGAGAGGAAGCTGTATGATC	GATATCTCTTGCCTCACAAC
	Hprt	ATGAGTACTTCAGGGATTTG	TGGCCTATAGGCTCATAGTG
	Arf	CTTGGTCACTGTGAGGATTCAG	CTATGCCCGTCGGTCTGGGC
	Ink4a	TCCGCTGCAGACAGACTGGCCAG	CTATGCCCGTCGGTCTGGGC
Genotyping	$Pcl2^{WT}$	GATGGTCAGATGGCTTGTTT	AGGTAGGTAAGTGGTGGTGC
	$Pcl2^{GT}$	GATGGTCAGATGGCTTGTTT	CAAGGCGATTAAGTTGGGTAACG
	$Pcl2^{\Delta}$	GGAACTCACTCTGTAGACCCTT	CAATGCTGGGTAGGCTGA

tion. Equal amounts of each sample were run on SDS-PAGE gels and subjected to Western blot analysis.

Generation of *Pcl2* mutant mice and ES cells. The gene-trapped embryonic stem (ES) cell line for the *Pcl2* locus (M016A06) was obtained from the European Mouse Mutant Archive (24). The endogenous *Pcl2* locus was disrupted by the insertion of a retroviral U3 β-galactosidase–Neo^r fusion gene (β-geo) gene trap vector. Its insertion into exon 4 results in disruption of the *Pcl2* open reading frame (ORF) (see Fig. S2 posted at http://web.rcai.riken.jp/en/paper_figs/Li_Supp_figs_rev3.pdf).

To generate deletion mutant mice, *Pcl2* homology arms, a 3.4-kb XbaI fragment that lies at the 5′ end of the exon 4 and a 2.4-kb KpnI/SalI fragment encompassing part of exon 5, were first introduced into the pPNT-loxP-Neo vector, in which the neomycin resistance gene (Neo^r) cassette was placed between two *loxP* sites (see Fig. S3 posted at the URL mentioned above). Homologous recombinants and germ line chimeras were isolated as described previously (1) (see Fig. S3B posted at the URL mentioned above). Heterozygous mutants were bred with CAG-Cre transgenic mice to delete the Neo^r cassette (54). $Pcl2^{+/\Delta}$ mice were backcrossed six times onto a C57BL/6 background. $Pcl2^{+/\Delta}$ mice were crossed with $Phc2^{+/-}$, $Mel18^{+/-}$, and $Suz12^{+/-}$ mice to generate compound mutants. All animal experiments were carried out according to the in-house guidelines for the care and use of laboratory animals of the RIKEN, Yokohama Institute, Japan.

Homozygous mutant ES cells were derived from respective mutant embryos as described previously (14). Primer pairs used for genotyping of these mutant alleles are listed in Table 2.

ChIP analysis. ChIP analysis was performed as described previously (18, 29). The primers used in this study are listed in Table 2.

ChIP-chip and ChIP-seq analyses. We used Agilent Mouse Promoter ChIP-on-Chip Set 244K with chromatin immunoprecipitation (ChIP-chip) using antibodies against H3K27me3, Ring1B, or Pcl2. We used probes showing significant intensities above background ($P < 10^{-7}$, Student's *t* test) and located from −4 kb to +4 kb of the transcription start site (TSS) of mouse genes. Methylated, ubiquitinated, or Ring1B- or Pcl2-binding positions were defined where the signal intensity of ChIP was 4 times (H3K27me3 and Pcl2) or 10 times (Ring1B) greater than that of input and when the statistical significance between the signals was less than 10^{-3}. To reduce noise in these assays, we removed detected probes that did not have significantly strong signals from input around the 500-bp region flanking their respective positions. ChIP followed by high-throughput sequencing (ChIP-seq) analysis was performed as described previously (37). Since this study is aimed to specifically elucidate the role of Pcl2 at the *Hox* and *Cdkn2a* genes, whole data sets of these analyses will be published elsewhere.

Skeletal, *in situ* RNA, and real-time PCR analyses. Skeletal preparations were made from perinatal mice, and cleared skeletons were analyzed under a stereomicroscope as described previously (1). *In situ* hybridization of tissue sections was performed as described previously (1). RNA extraction from ES cells, reverse transcription, and PCRs were performed as described previously (21). The expression of *Hox* and *Tbx3* genes was quantified relative to *Hprt* expression by real-time PCR analyses using an Mx3005P multiplex quantitative PCR system (Stratagene). Primer pairs used for reverse transcription-PCR (RT-PCR) analysis are listed in Table 2.

Cell culture of primary MEFs. Mouse embryonic fibroblasts (MEFs) were prepared as described previously (31). The *Mel18*-null, *Mel18/ARF*, and *Mel18/p53* double-null MEFs were routinely maintained with Dulbecco's modified Eagle's medium (DMEM) supplemented with 20% fetal bovine serum (FBS), 1× nonessential amino acids (Invitrogen), and 1× penicillin-streptomycin (Invitrogen). In modified 3T9 assays, cells were passaged at 3-day intervals and counted after trypsinization, and the number of cells per dish was recorded. A total of 1×10^6 cells were replated in 60-mm diameter dishes every 3 days (31). In growth rate assays, cells diluted to 2×10^4 cells per 60-mm diameter dish were plated in duplicate, and thereafter individual cultures harvested each day were counted. The Pcl2 expression retrovirus was prepared using a retrovirus packaging system (PlatE), according to the manufacturer's instructions, and transduced into immortalized MEF $Pcl2^{GT/GT}$ cells.

RESULTS

Identification of *Pcl2* transcripts and their products. Using database screening (GenBank accession number NM_013827.2), we identified a *Pcl2* transcript that is predicted to encode a protein containing a Tudor domain, two PHD fingers in the N-terminal region, and a chromo-like domain structure in the C-terminal region (Fig. 1A, upper scheme). In addition, we found a shorter transcript encoding a protein (AAI00341.1) lacking the Tudor domain (Fig. 1A, lower scheme). To elucidate the origin of the *Pcl2* isoforms, we examined the promoter and exon usage at the *Pcl2* locus through data sets obtained from recent genome-wide analyses for H3K4me3 occupancy and RNA transcription (see Fig. S1A posted at http://web.rcai.riken.jp/en/paper_figs/Li_Supp_figs_rev3.pdf) (44, 45). *Pcl2* appears to have a single predominant transcription start site, where there is extensive H3K4 trimethylation. We further found that usage of the 15 *Pcl2* exons was not necessarily uniform and that exons 2, 3, 5, and 11 were differentially expressed among brain, liver, and muscle. This analysis suggests that the *Pcl2*

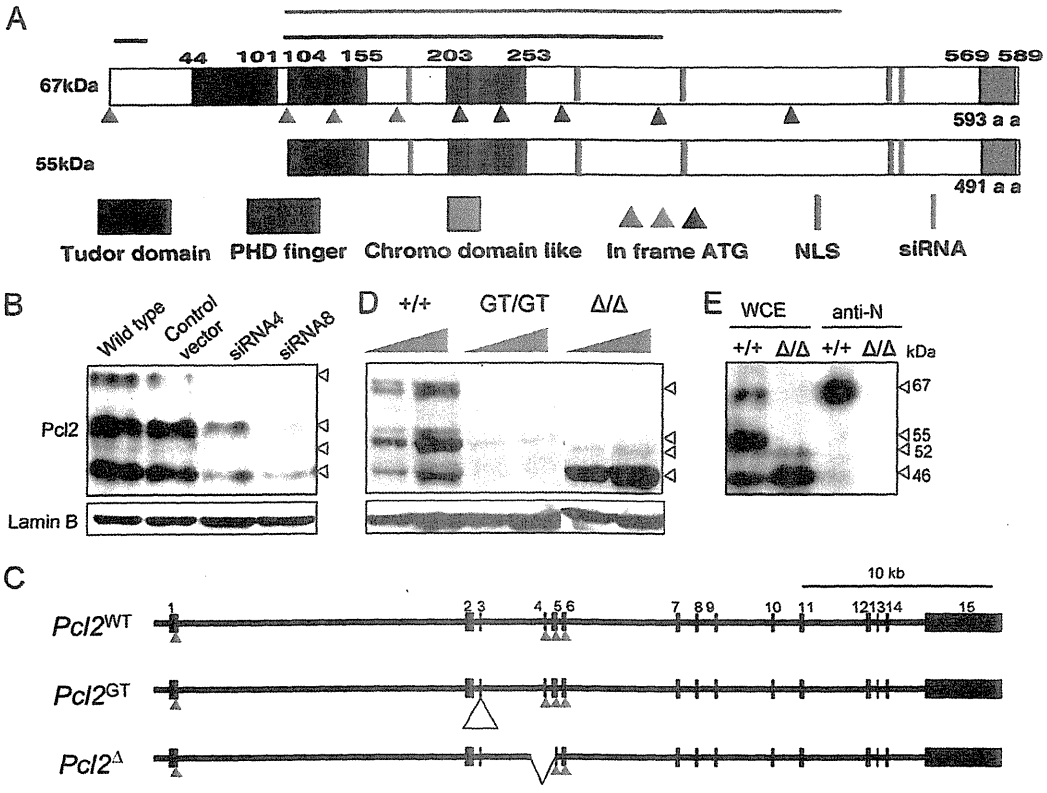

FIG. 1. Primary structure and the expression of mouse Pcl2 gene products. (A) Schematic representation of the two predicted Pcl2 isoforms. The black box corresponding to aa 44 to 101 representing the Tudor domain. The two dark blue boxes represent the PHD fingers. Three red vertical bars delineate the putative nuclear localization signals (NLS). A light blue box at aa 569 to 589 shows the chromo-like domain region at the C terminus. Positions for siRNA are demonstrated by light blue bars. The cDNA fragment isolated by two-hybrid screening for Mel18 interacting factors is shown by a green line at the top. The peptide and the fragment used to generate anti-Pcl2 antibodies are represented by two black lines. All ATG codons in the correct reading frame are indicated by colored triangles. Putative translation initiation codons for the 67- and 55-kDa isoforms are demarcated by red triangles, and those for 52- and 46-kDa isoforms are indicated by green triangles. (B) Expression of multiple Pcl2 isoforms in ES cells. The 67-, 55-, 52-, and 46-kDa bands were detected on Western blots of whole-cell lysates from wild-type ES cells using the Pcl2 MAb. The expression of *Pcl2* siRNA proportionally reduced the intensity of all four bands, whereas they were unaffected by the control siRNA. Lamin was used as a loading control. (C) Schematic representation of the genomic organization of $Pcl2^{GT}$ and $Pcl2^{\Delta}$ alleles. The $Pcl2^{GT}$ allele resulted from insertion of a gene trap vector (indicated by an open triangle) into exon 3. In the $Pcl2^{\Delta}$ allele, the genomic region encompassing the fourth intron to the middle of exon 5 is deleted. Genomic positions for putative translation initiation codons for the 67- and 55-kDa isoforms are indicated by red triangles, and those for 52- and 46-kDa isoforms are indicated by green triangles. (D) The 67-, 55-, 52-, and 46-kDa bands detected by the Pcl2 MAb were absent in $Pcl2^{GT/GT}$ ES cells, whereas only the 67- and 55-kDa bands were affected in $Pcl2^{\Delta/\Delta}$ ES cells. (E) Polyclonal antibodies against the N-terminal peptide of Pcl2 (anti-N) exclusively immunoprecipitated the 67-kDa isoform in the wild-type ES cells. WCE, whole-cell extract. The blot was probed with the Pcl2 MAb.

locus can give rise to several different transcripts, most likely due to alternative exon usage. We therefore inferred that the Pcl2 isoform lacking the Tudor domain could be produced from a transcript possessing exons 2 and 3 (see Fig. S1B posted at the URL mentioned above). In this case the nascent peptide initiating at the exon 1 start codon would prematurely terminate because of a frameshift; instead, productive translation would initiate at the start codon in exon 4, giving rise to a protein equivalent to AAI00341.1 (indicated by a green triangle in Fig. S1B posted at the URL mentioned above).

We then used Western blot analysis using a MAb produced against a GST-Pcl2 (aa 103 to 327) fusion protein to examine the expression of Pcl2 gene products. The MAb reproducibly detected strong bands of 67, 55, and 46 kDa and a much weaker 52-kDa band in whole-cell extracts of wild-type ES cells (Fig. 1B). To clarify whether these bands represent isoforms of Pcl2, we measured the effect of small interfering RNA (siRNA)-mediated knockdown of *Pcl2* in ES cells (Fig. 1A) on the appearance of the bands. Expression of two different siRNA constructs reduced the intensity of all four bands proportionally (Fig. 1B). These data indicate that *Pcl2* is expressed primarily as 67-, 55-, 52-, and 46-kDa isoforms.

To further elucidate the origin of the Pcl2 isoforms, we used two mutant alleles for *Pcl2*. Insertion of a gene-trap vector into exon 3 ($Pcl2^{GT}$) is expected to impair the expression of Pcl2 (Fig. 1C; see also Fig. S2 posted at http://web.rcai.riken.jp/en/paper_figs/Li_Supp_figs_rev3.pdf). In $Pcl2^{GT/GT}$ ES cells, we found this insertion diminished band intensities (Fig. 1D). In another allele, we deleted exon 4 and part of exon 5 by targeted mutagenesis ($Pcl2^{\Delta}$) (Fig. 1C; see also Fig. S3 posted at the URL mentioned above). This deletion resulted in the expression of truncated *Pcl2* transcripts in which exon 4 and 5 were skipped (X. Li, unpublished observations). These truncated

transcripts are predicted to encode a Pcl2 protein lacking the Tudor domain and the first PHD finger. Consistent with this prediction, the 67- and 55-kDa bands were abolished in $Pcl2^{\Delta/\Delta}$ ES cells. Therefore, the 67- and 55-kDa isoforms represent proteins with and without the Tudor domain, respectively (Fig. 1A). To validate this interpretation, we generated a polyclonal antibody against a synthetic polypeptide corresponding to part of the Pcl2 Tudor domain (aa 20 to 36). This antibody exclusively immunoprecipitated the 67-kDa band, confirming the presence of the Tudor domain in this isoform (Fig. 1E).

***Hox* repression by Pcl2.** *Hox* cluster genes are evolutionarily conserved targets for Polycomb repression during A-P specification of the axis. We thus examined axial skeletal development in $Pcl2^{GT/GT}$ and $Pcl2^{\Delta/\Delta}$ mice. Both mutant mice survived to birth; however, most of the $Pcl2^{GT/GT}$ mice died before weaning. In contrast, $Pcl2^{\Delta/\Delta}$ mice were viable and fertile. Although postnatal viabilities of the $Pcl2^{GT/GT}$ and $Pcl2^{\Delta/\Delta}$ mice were different, similar axial skeletal alterations that are characteristic of posterior transformations were observed in both mutants, as shown in a previous study (65) (Fig. 2A and B). Briefly, ectopic ribs that associated with the seventh cervical vertebra (C7) were frequently seen in $Pcl2^{GT/GT}$ and $Pcl2^{\Delta/\Delta}$ mice (indicated by arrows in Fig. 2A, frames b, c, e, f, n, and o). Consistent with this malformation, sternums were shifted anteriorly (indicated by brackets in Fig. 2A, frames b and c). The odontoid process, which is normally a characteristic of the second cervical vertebra (C2), was frequently associated with the first cervical vertebra (C1) in the mutants (indicated by red triangles in Fig. 2A, frames h to j). Axial skeletal changes indicating posterior transformations were also manifested at thoracolumbar and lumbosacral transitions of $Pcl2^{GT/GT}$ and $Pcl2^{\Delta/\Delta}$ mice (Fig. 2B). Therefore, Pcl2 proteins, particularly the 67- and/or 55-kDa isoforms, are required for A-P specifications of the axis, similar to other PcG proteins.

Next, we used *in situ* hybridization analysis to determine whether homeotic transformations in $Pcl2^{\Delta/\Delta}$ mice were accompanied by *Hox* gene derepression. The anterior boundaries of *Hoxb4*, *Hoxb6*, *Hoxb8*, and *Hoxd4* expression in the developing sclerotome were shifted cranially in $Pcl2^{\Delta/\Delta}$ embryos at 11.5 days postcoitus (dpc) (Fig. 2C). These results are consistent with homeotic transformations in the cervical and cervicothoracic boundary regions. We also found subtle but significant derepression of several *Hox* genes in $Pcl2^{\Delta/\Delta}$ ES cells (Fig. 2D). These results show that Pcl2 regulates *Hox* gene expression.

Pcl2 binds to *Hox* genes in a PRC2-dependent manner. Recent chromatin immunoprecipitation (ChIP) analyses revealed deposition of PRC2, PRC1, and H3K27me3 at the *Hox* cluster in developing embryos and ES cells. In parallel, *Drosophila* Pcl and human PHF1 were shown to be included in PRC2 in *Drosophila* and human cells, respectively (10, 47, 55, 56). Moreover, ChIP-seq studies reported significant overlap of genes bound by Pcl2 and Ezh2 in ES cells (41). These observations prompted us to hypothesize that Pcl2 mediates *Hox* repression via direct association with the *Hox* genes. By conventional ChIP assay using an anti-Pcl2 polyclonal antibody, we immunoprecipitated promoter regions of *Hoxb4*, *Hoxb6*, and *Hoxb8* from the wild-type ES cells but not from $Pcl2^{\Delta/\Delta}$ ES cells, which were used as a negative control (Fig. 3A). This result was further validated by ChIP-chip analysis using $Pcl2^{GT/GT}$ ES cells, which are reconstituted with the 67-kDa isoform of myc-tagged Pcl2. Here, an anti-myc antibody was used instead of the polyclonal antibody against the N-terminal peptide of Pcl2 (anti-N). In this experiment, too, we found considerable Pcl2 deposition around the transcription start sites (TSSs) of the *Hox* gene cluster, all of which were cooccupied by H3K27me3 and Ring1B (Fig. 3B; also D. Yamada and H. Koseki, unpublished data). Based on these results, we extended our analyses to the entire *Hoxd* cluster by ChIP-seq analysis using the anti-Pcl2 polyclonal antibody (Fig. 3C) (37). Indeed, the distribution profile of Pcl2 at the *Hoxd* cluster was similar to that of both Ezh2 and Ring1B. In particular, clear peaks that represented extensive binding of Pcl2, Ezh2, and Ring1B appeared concurrently around *Hoxd9*, *Hoxd10*, *Hoxd11*, *Hoxd12*, *Hoxd13*, and *Evx2*. Therefore, Pcl2 binds to *Hox* cluster genes, and its binding is correlated with local depositions of PRC2 and PRC1.

We went on to test whether Pcl2 expression and target binding depend on PRC2 because the expression of PRC2 components is known to be mutually dependent, and Pcl2 has already been reported as a PRC2-associated protein in mouse ES cells (21, 41, 63) (see Fig. S4 posted at http://web.rcai.riken.jp/en/paper_figs/Li_Supp_figs_rev3.pdf). In agreement with this view, we observed that the expression of Pcl2, as well as of Eed and Ezh2, was considerably decreased in $Suz12^{-/-}$ ES cells (Fig. 3D) (21). Particularly, the 67- and 55-kDa isoforms of Pcl2 were almost absent. We further used ChIP assays to confirm this result. Consistent with the reduction of Pcl2 expression in $Suz12^{-/-}$ ES cells, Pcl2 binding was almost nonexistent (Fig. 3E). It is worth noting that level of *Pcl2* transcripts was not proportionally altered in comparison to that of Pcl2 proteins in $Suz12^{-/-}$ ES cells (Fig. 3F). This suggests that Pcl2 expression is posttranscriptionally regulated in a PRC2-dependent manner. In contrast, the expression of Pcl2 and its binding to *Hox* genes were unaffected in $Ring1B^{-/-}$ ES cells (Fig. 4A and B). Moreover, the expression of PRC2 and PRC1 and their binding to *Hox* genes were not affected in $Pcl2^{\Delta/\Delta}$ ES cells (Fig. 4C and D). In summary, we conclude that Pcl2 binds to *Hox* genes in a PRC2-dependent manner.

***Hox* repression by Pcl2 involves its functional interactions with PRC2 and PRC1.** We went on to test whether *Hox* repression by Pcl2 involves its interactions with PRC2. It is well established that Polycomb components cooperate to mediate *Hox* repression via physical interactions. Indeed, *Drosophila Pcl* was isolated as an enhancer for the *extra sex combs* (*esc*) mutation (33). Therefore, we examined the interactions between *Pcl2* and *Suz12* (an essential component of PRC2) mutant alleles. Since *Suz12* homozygous mutants die around 8.5 dpc, heterozygous embryos were used. Notably, even the heterozygous mutants exhibited homeotic transformations of the axis, albeit to a lesser extent than $Pcl2^{\Delta/\Delta}$ mutants (Fig. 5A and B) (21). The skeletal phenotypes were compared between $Pcl2^{\Delta/\Delta}$ and $Pcl2^{\Delta/\Delta}$; $Suz12^{+/-}$ mice at the newborn stage, and significant differences were identified around the cervicothoracic boundary. Anterior tuberculums, which are characteristic of the C6 vertebra, were associated instead with the C5 in $Pcl2^{\Delta/\Delta}$; $Suz12^{+/-}$. The C7 vertebrae were associated with perfect ribs, which were attached to the anteriorly shifted sternum.

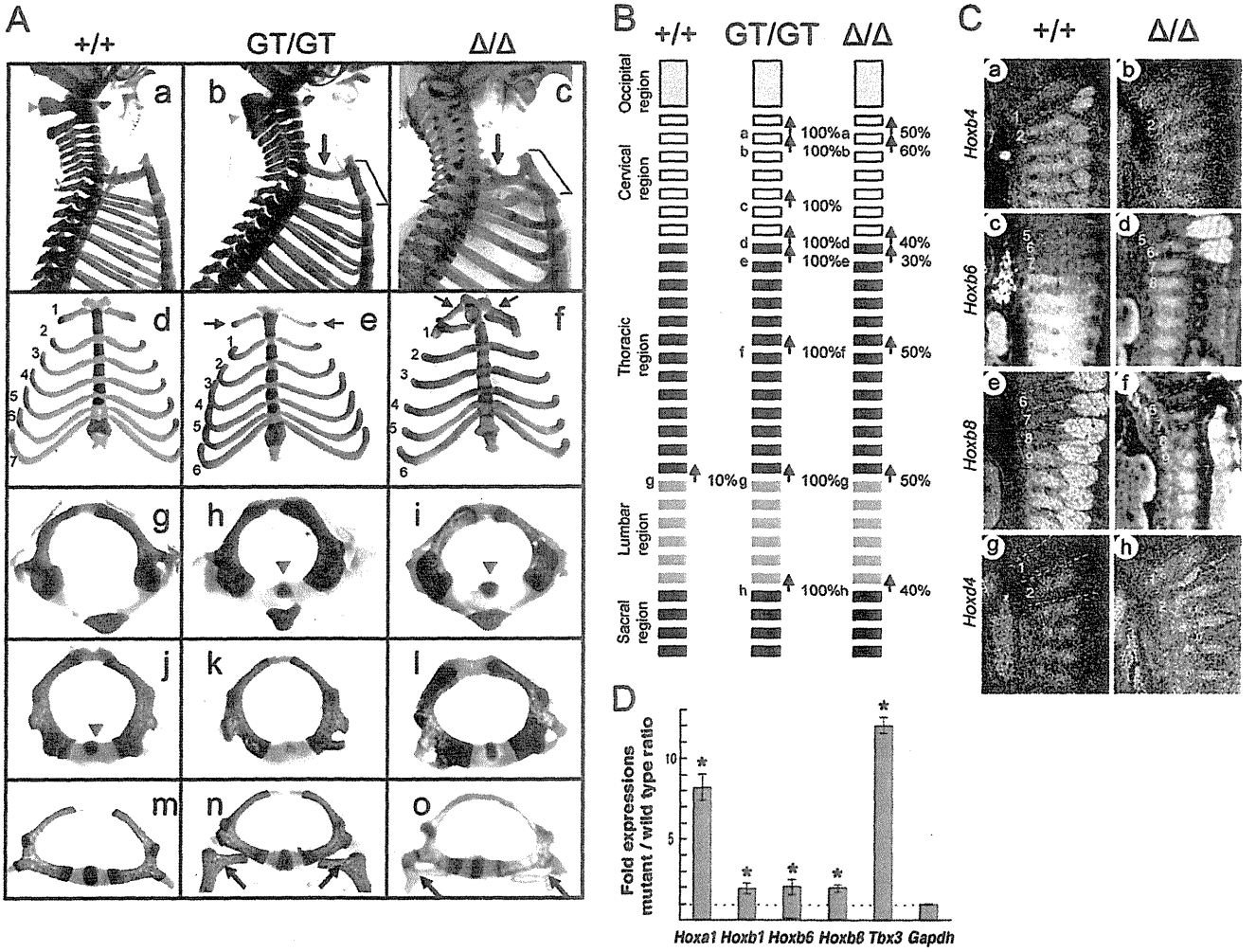

FIG. 2. Posterior transformation of the axis in $Pcl2^{GT/GT}$ and $Pcl2^{\Delta/\Delta}$ mutants. (A) Skeletal alterations in $Pcl2^{GT/GT}$ (GT/GT) and $Pcl2^{\Delta/\Delta}$ (Δ/Δ) mutants. (Frames a, b, and c) Lateral views of the upper part of the vertebral column are shown. Yellow arrowheads indicate the first cervical vertebra. The arrows and brackets in frames b and c indicate the ectopic ribs associated with C7 and the anteriorly shifted sternum, respectively. (Frames d, e, and f) Ventral views of the rib cages are shown. In frames e and f, the ectopic ribs associated with C7 are indicated by arrows. (Frames g, h, and i) Overviews of isolated C1 vertebrae. Odontoid processes fused with C1 are indicated by arrowheads in frames h and i. (Frames j, k, and l) Overviews of isolated C2 vertebrae. The odontoid process is indicated by an arrowhead in frame j. (Frames m, n, and o) Overviews of isolated C7 vertebrae. Ectopic ribs are indicated by arrows in frames n and o. (B) Schematic summary of the axial homeotic transformations in $Pcl2^{GT/GT}$ and $Pcl2^{\Delta/\Delta}$ mice. The following parameters, identified by letters on the figure, were scored, and the frequency of each alteration is indicated: C1 → C2, presence of the odontoid process on the C1 vertebra (a); C2 → C3, lack of the odontoid process from the C2 vertebra (b); C5 → C6, appearance of anterior tuberculum (c); C7 → T1, appearance of cervical ribs on C7 (d); T1 → T2, prominent spinous process on T1 (e); T7 → T8, dissociation of seventh rib from the sternum (f); T13 → L1, loss of the rib on 20th vertebra (g); lumbar vertebra 5 (L5) or L6 → sacral vertebra 1 (S1), formation of the sacroiliac joint in 25th or 26th vertebra (h). (C) Expression of *Hox* genes in 11.5-dpc wild-type and $Pcl2^{\Delta/\Delta}$ embryos. The expression of *Hoxb4* (a and b), *Hoxb6* (c and d), *Hoxb8* (e and f), and *Hoxd4* (g and h) is shown. Prevertebrae are numbered starting from the proatlas, and dotted lines indicate the segment boundaries. (D) Derepression of *Hox* genes in $Pcl2^{\Delta/\Delta}$ ES cells. *Hoxa1*, *Hoxb4*, *Hoxb6*, *Hoxb8*, and *Tbx3* were derepressed in $Pcl2^{\Delta/\Delta}$ ES cells compared to the wild-type controls by real-time PCR. Fold expression of respective genes in $Pcl2^{\Delta/\Delta}$ ES cells compared to that of the wild type is shown by bars. Statistically significant differences are indicated by asterisks.

A prominent spinous process, which appeared on thoracic vertebra 2 (T2) in the wild-type, $Suz12^{+/-}$, and $Pcl2^{\Delta/\Delta}$ pups, was frequently associated with the T1 in $Pcl2^{\Delta/\Delta}$; $Suz12^{+/-}$ mutants. In summary, heterozygous loss of *Suz12* synergistically enhanced the homeotic transformations of *Pcl2* single mutants. Taken together, we conclude that *Hox* repression by Pcl2 involves its interaction with PRC2. Since Pcl and PHF1 are known to enhance the catalytic activity of PRC2, we inferred that Pcl2 contributes to *Hox* repression by regulating PRC2 activity. We did not, however, observe extensive changes in global and local levels of H3K27me3 in $Pcl2^{\Delta/\Delta}$ ES cells (Fig. 4C and D). Supporting this observation, binding of Ring1B to *Hox* genes was not changed despite *Hox* derepression in ES cells. As the molecular mechanisms that underlie Pcl2-dependent regulation of PRC2 are still unclear, we speculated that Pcl2-mediated *Hox* repression might involve PRC1.

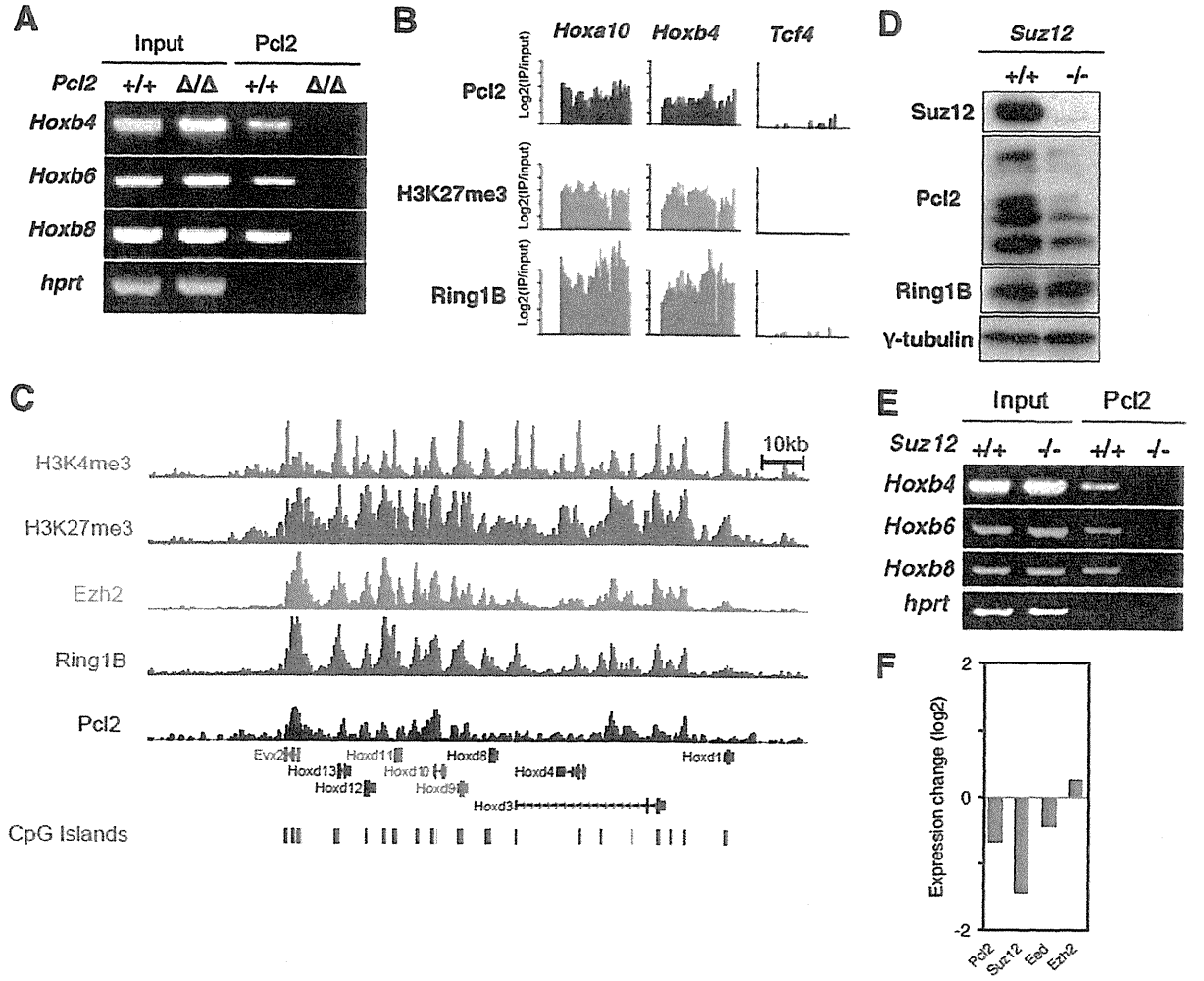

FIG. 3. PRC2-dependent binding of Pcl2 to *Hox* genes. (A) Pcl2 association at *Hox* promoter regions revealed by conventional ChIP assay using anti-N polyclonal in $Pcl2^{+/+}$ (+/+) and $Pcl2^{\Delta/\Delta}$ (Δ/Δ) ES cells. For the input, genomic DNA extracted from the original whole-cell lysate equivalent to 1/40 of the volume used for the ChIP analysis was subjected to PCR; the *hprt* gene was used as a negative control. (B) The distribution of Pcl2, H3K27me3, and Ring1B at the promoter regions of the genes in ES cells. Agilent mouse promoter ChIP-on-Chip Sets 244K were used for *Hoxa10*, *Hoxb4*, and *Tcf4* promoter region analysis. (C) ChIP-seq binding patterns for *Evx2* and *Hoxd* loci are shown for H3K4me3, H3K27me3, Ezh2, Ring1B, and Pcl2 in ES cells. CpG islands are shown as green bars (below). (D) Impact of Suz12 deficiency on the expression of Pcl2. The expression of Suz12, Pcl2, Rnf2, and γ-tubulin in $Suz12^{+/+}$ (+/+) and $Suz12^{-/-}$ (−/−) ES cells as revealed by Western blotting. (E) Pcl2 association at *Hox* promoter regions in $Suz12^{+/+}$ and $Suz12^{-/-}$ ES cells. For the input, genomic DNA extracted from the original whole-cell lysate equivalent to 1/40 of the volume used for the ChIP analysis was subjected to PCR; the *hprt* gene was used as a negative control. (F) Expression changes of *Pcl2*, *Suz12*, *Eed*, and *Ezh2* in $Suz12^{-/-}$ ES cells. Expression changes of *Pcl2*, *Suz12*, *Eed*, and *Ezh2* in $Suz12^{-/-}$ ES cells were revealed by microarray analysis using Affymetrix Mouse 430.2. Detected signals were normalized using a quantile normalization method, and only signals having significant intensity from background were counted. The average signal intensity of respective genes in $Suz12^{-/-}$ and wild-type ES cells was calculated, and the log ratios of $Suz12^{-/-}$ against wild type are shown by bars.

We thus examined whether the *Pcl2* mutation functionally interacts with mutations in genes encoding PRC1 components since previous reports have shown that compound mutants of PRC1 genes have a more severe phenotype than single mutants, suggesting the importance of such cooperativity (2, 6). We therefore compared the axial skeletal abnormalities in $Pcl2^{\Delta/\Delta}$; $Mel18^{-/-}$ and $Pcl2^{\Delta/\Delta}$; $Mel18^{+/+}$ mice. Notably, no viable $Pcl2^{\Delta/\Delta}$; $Mel18^{-/-}$ mice were seen at the perinatal stage, whereas the respective single homozygotes ($Pcl2^{\Delta/\Delta}$; $Mel18^{+/+}$ and $Pcl2^{+/+}$; $Mel18^{-/-}$) survived. Because of this, the skeletal phenotypes were examined at 16.5 dpc. $Mel18^{-/-}$ fetuses had phenotypes that were nearly identical to those in the $Pcl2^{\Delta/\Delta}$ fetuses, as reported previously (1). The $Pcl2^{\Delta/\Delta}$; $Mel18^{-/-}$ double mutants showed more stringent transformations than either of the single mutants (Fig. 5C and D). Occipital bones were segmented, resulting in the formation of an ectopic arch. The C1 vertebrae were identical to the wild-type C2, and perfect ribs bridged an anteriorly shifted sternum and the C7. Interestingly, a hole reproducibly appeared at the central region of the scapula of $Pcl2^{\Delta/\Delta}$; $Mel18^{-/-}$ mice, which was not seen in either of the single mutants. A similar synthetic defect in the scapula has been reported in $Mel18^{-/-}$; $Phc2^{-/-}$ and $Mel18^{-/-}$; $Bmi1^{+/-}$ mice due to the combined effects of the respective mutations (2, 28). Taken together, the genetic in-